80p

Code 1 N64-27388

CR-56316 Cat 15

THEORETICAL ANALYSIS OF OPERATIONAL CHARACTERISTICS OF MICROMETEOROID CAPACITOR DETECTOR

prepared for

Instruments Research Division
Langley Research Center, NASA
Hampton, Virginia

April 1964

(Prepared under Contract NAS1-3343 by the
Solid State Laboratory of the
Research Triangle Institute, Durham, North Carolina)

OTS PRICE

OX $ 7.60 ph

ROFILM $ _____

FOREWORD

This report was prepared by the Research Triangle Institute, Durham, North Carolina, on NASA Contract NAS1-334, "Theoretical Analysis of Operational Characteristics of Micrometeoroid Capacitor Detectors." This work was administered under the direction of the Instrument Research Division at Langley Research Center. Charles C. Laney was project engineer for NASA.

The studies presented began in September 1963 and were concluded in March 1964 and were performed by the Solid State Laboratory of the Research Triangle Institute under the general direction of R. M. Burger. While L. K. Monteith and A. M. Smith were the authors of this report, numerous persons have contributed the ideas, analysis and conclusions as a result of three meetings of an RTI-NASA-University panel. The detector problem was approached on a group basis in an attempt to cover many points rapidly. This panel group consisted of selected RTI, university faculty and NASA representatives who have knowledge in one or more of the problem areas. The university faculty and NASA representatives in attendance at one or more meetings are listed below:

NASA	University Faculty
C. Laney - LRC	Dr. Fowler - Duke
W. Kinard - LRC	Dr. McDonald - N. C. State
Miss Smith - MSFC	Dr. Owen - Duke
J. Siviter - LRC	Dr. Palmetier - UNC
J. Broderick - LRC	Dr. Slifkin - UNC

TABLE OF CONTENTS

Section		Page
1.	INTRODUCTION	1
2.	SPACE ENVIRONMENT	2
3.	EXPERIMENTALLY OBSERVED IMPACE PHENOMENA OCCURRING ON PENETRATION OF A CAPACITOR-TYPE DETECTOR BY A HIGH-VELOCITY PROJECTILE	6
4.	MODEL OF THE IMPACT OF A PROJECTILE ON A MICROMETEOROID DETECTOR	9
5.	MECHANISM OF CAPACITOR DISCHARGE	22
6.	CORRELATION OF EXPERIMENTAL OBSERVATIONS WITH THE THEORETICAL MODEL	28
7.	AMBIGUOUS SIGNAL GENERATION	32
8.	ELECTRON PENETRATION OF ALUMINUM	35
9.	RADIATION EFFECTS IN MYLAR	48
10.	INTERNAL SPACE CHARGE BUILDUP AND ELECTRICAL BREAKDOWN	50
11.	CORRELATION OF DATA WITH THEORETICAL MODEL	58
12.	SUMMARY	60
13.	RECOMMENDATIONS	62
APPENDIX A		64
APPENDIX B		66
APPENDIX C		68
REFERENCES		74

LIST OF ILLUSTRATIONS

Figure		Page
1	Frequency distribution and possible energy range as functions of meteorite mass	1
2	Electron flux at peak of outer radiation belt where the two curves indicate the range of values either predicted or determined experimentally	5
3	Estimated wave patterns in projectile and micrometeoroid detector	10
4	One-dimensional situation immediately after impact of projectile on micrometeoroid detector	11
5	Initial interface pressures in one-dimensional impact	16
6	Initial capacitor temperature in one-dimensional impact	17
7	Initial projectile temperature in one-dimensional impact	18
8	Typical conductance-time trace of a dense metal-like plasma	20
9	Static pressure P_a required to initiate elector-mechanical breakdown of 0.25 mil Mylar dielectric capacitor with applied voltage V	23
10	Equivalent circuit for capacitor discharge due to micrometeoroid impact where it is explicitly assumed that $V_c = V_a$ at time t = 0 and R_B is the discharge resistance through the capacitor	25
11	Arrangement of capacitor for electron radiation with evaporated aluminum electrode grounded	33
12	Arrangement of capacitor for electron radiation with 1 mil aluminum grounded	33
13	Capacitor type micrometeoroid detector tested at Ling Temco Vought	34
14	The bremsstrahlung intensity per frequency interval from a thick target	36
15	Mass attenuation coefficients for photons in aluminum	37
16	Energy spectrum of secondary electrons for aluminum resulting from a primary beam of energetic electrons	39

LIST OF ILLUSTRATIONS (Continued)

Figure		Page
17	Yield vs energy data obtained with 1.8 mg/cm^2 and 5.2 mg/cm^2 Al target electrodes	40
18	Range energy for monoenergetic electrons in aluminum	41
19	Most probable energy loss for electrons in 1 mil Al and 1/4 mil Mylar	44
20	Most probable energy and FWHM of energy spectrum through 1 mil Al with most probable energy loss in 1/4 mil Mylar	45
21	Straggling distribution for electrons in three thicknesses of Be where the absicissa is in arbitrary units and the ordinate is in counts per minute. The thicknesses are in mg/cm^2. The energy of the incident electrons is 624 kev.	46
22	Assumed charge distribution in traps with boundaries 1 and 2 grounded	51
23	Maximum built-in field for a uniform electron density	53
C-1	Energy pass band for the cylindrical transmission line model with 3 transmission path lengths of 0.1, 1, and 10 cm	71
C-2	Discharge signal originating at penetration radius r_0	72
C-3	Power density spectrum for an exponential signal shown in Figure 2	73

1. INTRODUCTION

The purpose of this study was to analyze the use of a structure in the form of a capacitor for the counting of micrometeoroids which penetrate and leave holes. The reasons for NASA interest in such a detector are obvious. What is not obvious is the phenomenological explanation of the detection process and whether such a detector will operate so as to give the desired information in a space enviornment. The detector structure which has been considered is a capacitor consisting of a 1-mil aluminum or stainless steel electrode, 1/4 mill polymer dielectric, and an evaporated metal counter-electrode. The micrometeoroids will impact against the 1 mil electrode. With a voltage across the capacitor the impacting micrometeoroid can initiate a discharge of the capacitor and a recharge through a load resistor. Appropriate detection circuits will count the number of discharge-recharge pulses, hence the number of impacts. The simplicity of the capacitor structure and the possibility of constructing large sensing areas make it very attractive for detecting micrometeoroids. However, to interpret the data received from a space experiment with a high degree of confidence, the operational characteristics of the capacitor structure must be analyzed and experimentally verified in a simulated space environment. The analysis has been divided into two main areas of investigation. These are (1) a study of the signal generation mechanism on micrometeoroid impact (2) a study of possible ambiguous signal generation due to space radiation.

The study of the impact phenomena occuring on penetration of a micrometeoroid detector by a high-velocity projectile was carried out by formulating a model for the impact process and then using this model to suggest possible mechanisms of capacitor discharge when penetrated by a high-velocity projectile. Finally an attempt was made to correlate the experimental observations of the NASA with the proposed model.

To study the effects of space radiation upon the operational characteristics of the detector the following topics have to be considered:

1. Charged particle penetration of solids and subsequent energy losses;
2. Electron trapping in solids which result in a space charge buildup;
3. The liberation of trapped electrons through breakdown induced by the electric field resulting from the space charge;
4. Radiation induced changes in physical and chemical properties of solids.

The possibility of ambigious signal generation has been predicted on the available data from the literature pertaining to each of these topics. Extrapolations from fundamental studies on the physical, chemical and electrical properties of the materials which make up the sensor were used in an attempt to analyze and understand the observations by NASA when the micrometeoroid detector was exposed to radiation.

2. SPACE ENVIRONMENT

Detailed surveys of the environmental factors constituting the space environment have appeared in recent publications.[1,2,3] Those factors used in analyzing the operational characteristics of a capacitor structure as a micrometeoroid detector have been included to provide a means of determining their relative importance. The micrometeoroid environment is of primary importance and has been characterized by the frequency distribution and possible energy range shown in Figure 1. This simple distribution agrees within several orders of magnitude with the data obtained from rocket and satellite space experiments.[3] However this distribution is an average which does not consider the spatial distribution of micrometeoroids. Data for a particle mass of 10^{-9} grams indicate that the flux depends inversely on the altitude for the range of 10^3 to 10^6 km.[3]

In addition to the micrometeoroid environment the sensor will be exposed to a variety of radiations which may influence its operation. Electrons, protons, gamma rays, and ions are believed to be the more important. Again, there is voluminous data about the radiation aspect of the space environment and only the data pertinent to the analysis of the sensor are included. The total energy given up to the sensor by the various radiation components is important in determining the expected degradation of the physical and electrical properties of the dielectric. Thus one is interested in the ionizations and atomic displacements which result from the expected radiation dosage. From Table 1, the relative importance of the various radiation sources can be determined. In addition it is pertinent to this analysis to know the electron distribution in the Van Allen Belts. There has been much controversy over the actual flux, however Figure 2 shows the range of distributions which have been considered. Recent experiments indicate that the equilibrium value of electron flux may even be less than either of these estimates.[3] The effect of radiation upon the physical and electrical properties of the materials used to construct the capacitor sensor are available. However these effects are not easily correlated with the capacitor device parameters. Therefore the primary consideration in this analysis is whether these effects can lead to error counts or degradation of the detector and not the cause-effect relationship associated with radiation damage in solids.

Table 1. Radiation Dosages: Ionization and Displacement Produced by Atomic Particles in Space[2]

Radiation	Energy ev	Range gm/cm^2	Ionization, erg/g-yr Through 1 mg/cm^2	Ionization, erg/g-yr Through 1 g/cm^2
Inner radiation belt				
Protons	10^3(?) - 7×10^8	10^{-6}(?) - 10^3	10^{11}	10^7
Electrons	$<2 \times 10^4$ - 1×10^6	10^{-3} - 10^0	10^{14}	0
Bremsstrahlung	$<2 \times 10^4$ - 1×10^6	10^{-1} - 10^1	10^7	10^7 - 10^8
Total			10^{14}	10^7 - 10^8
Due principally to[a]			e	γ, p
Outer radiation belt				
Electrons	2×10^4 - 5×10^6	10^{-3} - 10^0	10^{13} - 10^{15}	10^5
Bremsstrahlung	2×10^4 - 5×10^6	$10^{-1} \times 10^1$	10^7 - 10^9	10^6 - 10^8
Total			10^{13} - 10^{15}	10^6 - 10^8
Due principally to			e	γ
Solar flare high energy particles				
Protons	2×10^7 - 10^9	10^0 - 10^3	10^5 - 10^6	10^4 - 10^5
Electrons	$\sim 5 \times 10^4$	10^{-2}	10^7 - 10^9(?)	0
Bremsstrahlung	$\sim 5 \times 10^4$	10^0 - 10^1	10^2 - 10^4(?)	10^2 - 10^4(?)
Total			10^7 - 10^9(?)	10^4 - 10^5
Due principally to			e(?)	p(?)
Solar flare low energy particles				
Protons	5×10^2 - 2×10^4	10^{-6}(?) - 10^{-5}(?)	0	0
Electrons	2×10^{-1} - 10^1	10^{-8}	0	0
Bremsstrahlung	2×10^{-1} - 10^1	10^{-6}(?) - 10^3	0	0
Steady solar emission				
Protons	10^0 - 10^3	10^{-8} - 10^{-6}(?)	0	0
Electrons	10^0	10^{-8}	0	0
Bremsstrahlung	10^0	10^{-7}	0	0
Cosmic rays				
Protons	10^8 - 10^{19}	$>10^{-1}$	10^2 - 10^3	10^2 - 10^3

[a] e electron; p proton; γ bremsstrahlung photon

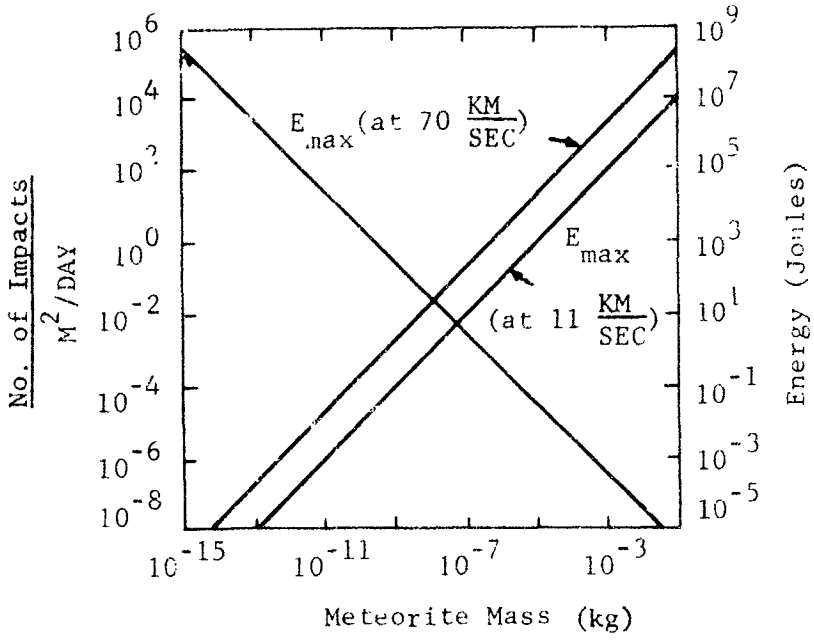

Figure 1. Frequency distribution and possible energy range as functions[4] of meteorite mass

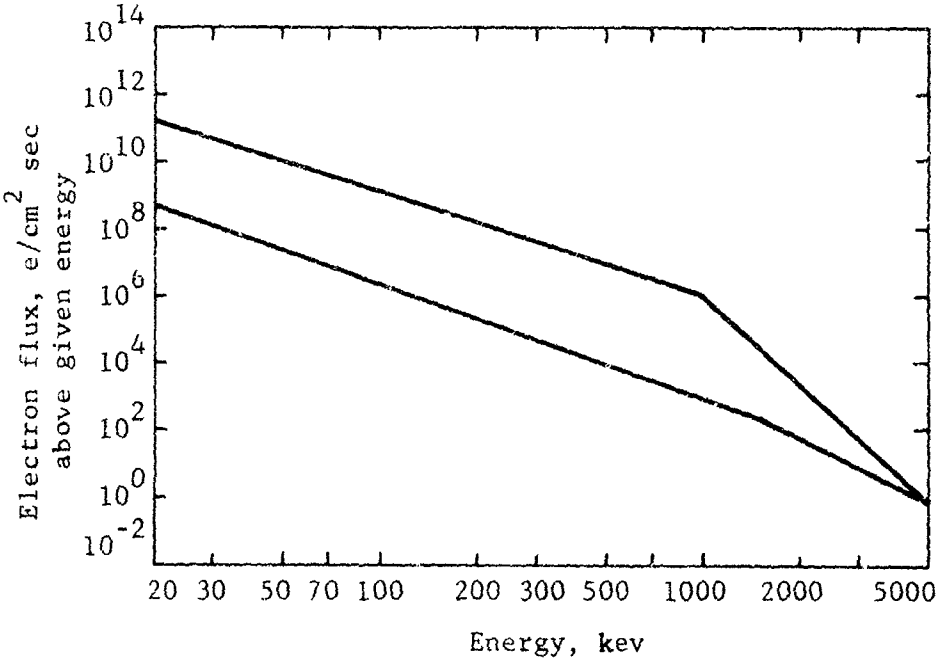

Figure 2. Electron flux at peak of outer radiation belt[2] where the two curves indicate the range of values either predicted or determined experimentally

3. EXPERIMENTALLY OBSERVED IMPACT PHENOMENA OCCURRING ON PENETRATION OF A CAPACITOR-TYPE DETECTOR BY A HIGH-VELOCITY PROJECTILE

Experimental investigations of high-velocity projectiles penetrating a capacitor-type micrometeoroid detector have been conducted under laboratory conditions by Langley and Lewis Research Center of NASA. The pertinent results of these investigations were presented at the meetings of the RTI-NASA-University panel. These results are reported below.

The results of Lewis Research Center's experiments, as reported by Frank Pollack, were obtained for projectiles impacting a coincidence type micrometeoroid detector. This sensor was formed by bonding a thin film of Mylar to both sides of a stainless steel panel and then vapor-depositing a thin aluminum electrode on top of the Mylar. With a voltage across the capacitor structure, metallic and non-metallic particles ranging in size from 1 to 350 microns in diameter were fired at the sensor at velocities ranging from 7000 ft/sec to 45,000 ft/sec. These firings were conducted in both ambient air and in a vacuum as low as 10^{-5} torr. When a projectile penetrated all or part of the sensor structure a capacitor discharge was initiated. The research performed at Lewis Research Center indicated that for voltages between 100 and 150 volts, capacitor discharge was probably due to dielectric breakdown resulting from the high field (1.5×10^6 v/cm) and structural damage to the capacitor due to the penetrating particle. Their results indicated that the characteristics of the discharge pulse (discharge voltage, V_d) were proportional to the capacitance and series resistance in the discharge path and that V_d was normally less than the applied voltage, V_c. It was found that the amplitude of the discharge pulse was proportional to the thickness of the aluminum electrode. Increasing the electrode thickness increased V_d. Also for tests conducted in a vacuum the magnitude of V_d was found to be 10 - 15% larger than for tests conducted in ambient air. The experimental results also indicated that a positive polarity on the outside aluminum electrode and a negative ground on the steel plate enhanced the discharge mechanism of the sensor.

Experiments conducted by the group at Langley Research Center, as reported by Bill Kinard, differed from those of Lewis Research Center in that lower values of applied voltage (2 - 100 volts) were used. The capacitor structure first tested consisted of 25 microinch aluminum electrodes bonded to both sides of an 0.25 mil Mylar dielectric. When 0.22 caliber nylon cylinders were fired at this structure no discharge was observed. However when the capacitor was backed by a bakelite plate a discharge was observed. The applied voltage was varied from 2 to 100 volts during this set of firings but no effect on the discharge voltage was noted. However it was noted from these experiments that the discharge pulse amplitude depended upon the velocity of the penetrating particle and that $V_d \longrightarrow V_c$ for velocities in the range of 10^4 ft/sec. For velocities below this limiting value, the discharge voltage ranged over 3 to 4 orders of magnitude as the velocity of the particle was

increased. It was also observed that as the size of the particle decreased, the velocity had to be increased to trigger the discharge. Spectral measurements taken during the impact indicated that there was ionization of both the projectile and the target. Iron fragments have also been used to discharge the capacitor.

A similar capacitor structure with a front aluminum electrode of 1 mil thickness was also tested. It was observed that the peak discharge voltage was reached in less than 1 μsec. Tests conducted in ambient air and a vacuum indicated that the capacitor was more likely to discharge in ambient air when penetrated. When the capacitor discharged, the value of V_d ranged from 0 to V_c but with bakelite backup palte V_d equalled V_c. Photographs of the impact were taken in the dark and a bright flare of visible light accompanied the penetration of the projectiles. The major portion of the light seemed to emanate from the incident surface with only a minor flare at the exit hole. The duration of the flash was measured by a photomultiplier tube. Also the output of the photomultiplier tube correlated with the bottoming of the discharge pulse.

Results of further experiments conducted at Langley Research Center were reported by Jim Siviter. These tests were conducted on a structure formed by vapor-depositing aluminum on both sides of a Mylar dielectric. Pellets of 1/16 to 1/8 inch diameter were fired at this sensor at velocities ranging from 8000 ft/sec to 16,000 ft/sec. Up to 8000 ft/sec the capacitor did not discharge. It was found that with an applied voltage across the capacitor of 5 to 15 volts the discharge signal was approximately 50% of the applied voltage while for an applied voltage of 15 to 90 volts the discharge signal was approximately 60 to 70% of the applied voltage. No effect of projectile diameter was noted. There also appeared to be no noticeable difference between conducting and non-conducting particles.

Tests were also conducted on a capacitor structure which consisted of a 1 mil stainless steel front electrode, a 1/4 mil Mylar dielectric, and a vapor-deposited aluminum back electrode. When steel projectiles of 1/16 to 1/8 inch diameter were fired at this capacitor structure in the velocity range of 8000 to 16,000 ft/sec it was found that the discharge signal was approximately 15% larger than for the previous capacitor structure with the vapor deposited aluminum front plate.

J. Broderick of Langley Research Center reported on tests conducted at North American Aviation on a capacitor structure consisting of a 1 mil stainless steel front electrode, a 1/4 mil Mylar dielectric and a 12 microinch copper back electrode. The average velocity of the impacting particles was approximately 9.5 km/sec. Fifteen tests each were conducted at values of applied voltage of 15, 30, 60 and 120 volts. It was found that the average discharge voltage was proportional to the applied voltage and that the ratio of the standard deviation to the applied voltage remained constant for each value of applied voltage. When the applied voltage was 80 or above, the discharge voltage approached the applied voltage. It was also noted that when similar tests were

conducted on a capacitor with 0.25 microinch aluminum front electrode, the light flash was less intense than for a 1 mil stainless steel electrode. It was also observed that the light flash was more intense at 15 volts than at the higher applied voltages. However, the intensity of the light flash was approximately the same for the applied voltages greater than 15 volts.

4. MODEL OF THE IMPACT OF A PROJECTILE ON A MICROMETEOROID DETECTOR

In order to analyze the problem of penetration of a thin film capacitor-type micrometeoroid detector by a high velocity projectile, a model will be assumed which allows the use of one-dimensional shock wave theory to predict the impact shock-induced conditions. Since the capacitor is thin, then it is a reasonable assumption that the conditions occurring initially on impact will be felt across the capacitor structure and hence the breakdown mechanism of the capacitor will be generated by the impact induced conditions.

In any impact model the displacement phenomena are initiated by shocks generated at the instant of impact. These shocks are then propagated through both of the colliding bodies. It is well known that hydrodynamic shock wave theory gives a good estimate of the impact induced properties in the initial stages of impact. Hence the theoretical model is based on a fluid model since the shock pressures generated on impact are at least an order of magnitude greater than the yield stresses of the colliding bodies.

The attack on the micrometeoroid detector penetration problem will consist of determining the initial impact-induced thermodynamic states on the basis of one-dimensional shock wave theory and then relating these conditions to a mechanism which causes capacitor discharge.

Consider a cylindrical projectile impacting the front plate of the capacitor at velocity v_o. The estimated wave pattern shortly after impact is shown in Figure 3. Two shock waves S_p and S_c have propagated away from the interface I. The fact that the projectile is finite in diameter means that rarefaction waves R_p and R_c will be transmitted toward the axis of symmetry. The formation of these rarefaction waves results in ejection of both projectile and front electrode material in a rearward direction. Now as the impact shocks S_p and S_c travel from the point of impact they will, in general, be diffracted. However, for a thin capacitor front plate, diffraction effects may be neglected and a one-dimensional model assumed where the situation in the one-dimensional region immediately after impact is shown in Figure 4. In this figure and subsequent analyses all velocities are measured with respect to a set of coordinates fixed in the capacitor.

In Figure 4 a transmitted shock S_c proceeds into the capacitor at velocity w_c while a reflected shock S_p proceeds into the projectile at velocity w_p. The physical formation of these shocks is such as to establish the contact interface in the ideal mechanical model where it is assumed that no penetration mixing of projectile and capacitor material occurs. Thus at the interface, the capacitor shock accelerates the front plate material to a velocity u_c equal to the decreased projectile velocity, $v_o - u_p$, resulting from shock S_p. This is defined analytically by the relation

$$u_c = v_o - u_p \tag{1}$$

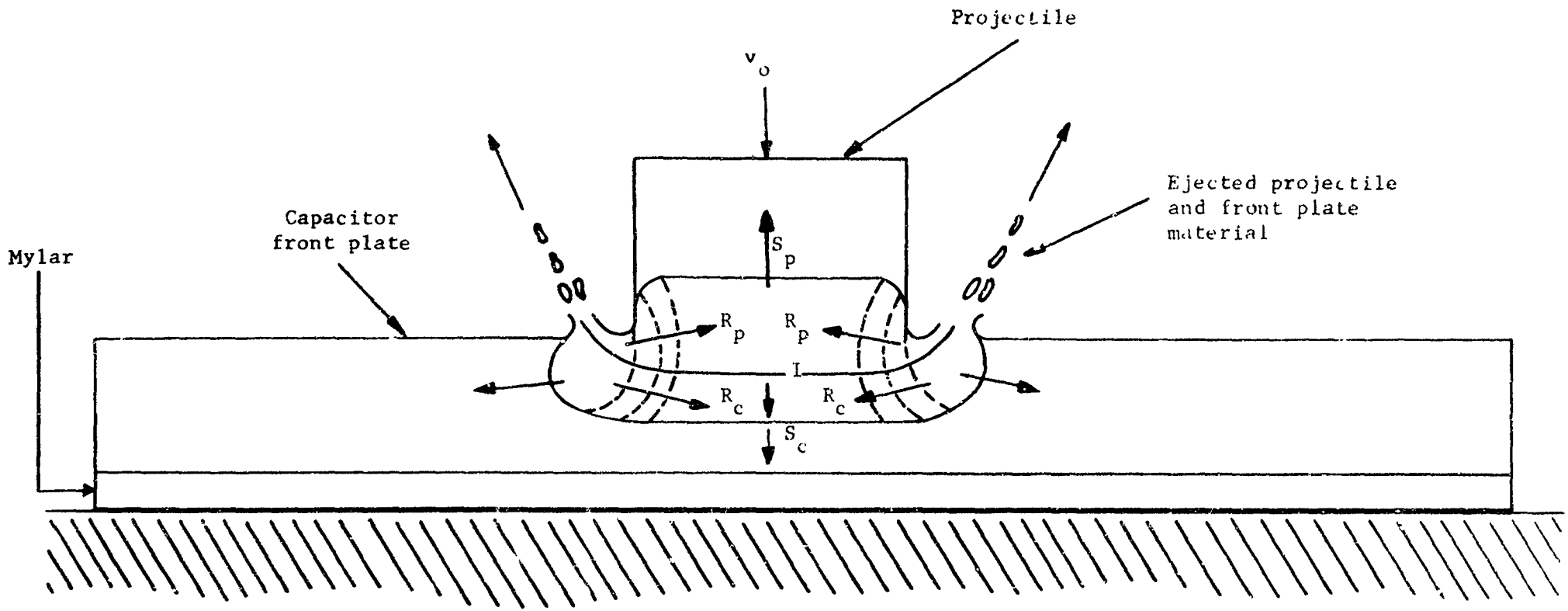

Figure 3. Estimated wave patterns in projectile and micrometeoroid detector

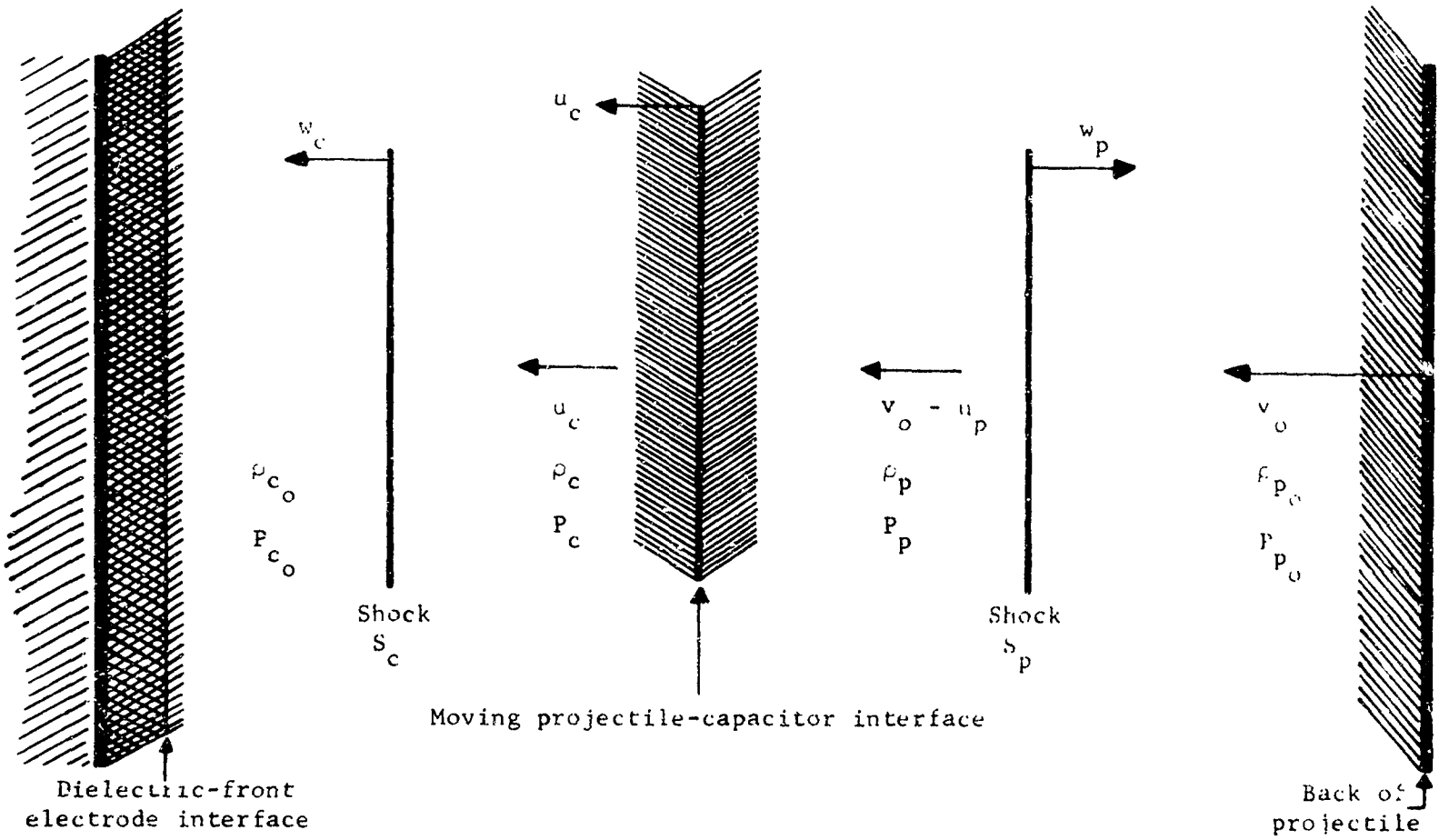

Figure 4. One-dimensional situation immediately after impact of projectile on micrometeoroid detector

which simply says that the projectile and capacitor remain in contact. The pressures acting on the contact interface are equal so

$$P_c = P_p \ . \tag{2}$$

The contact interface is then separating the capacitor and projectile material and travelling to the right at the particle velocity, u_c. In many instances all these waves will travel at considerably less than the impact velocity in which case all will be swept to the right with respect to an axis system fixed in the capacitor.

Thus, in this model, it is seen that on impact the kinetic energy is transferred partially into the kinetic energy of the affected regions of the capacitor and partially into thermal energy of both pellet and capacitor material. The energy transfer is effected through the transmitted and reflected shock waves.

The analysis of the shock model in Figure 4 is based on the assumption that the media involved are compressible and non-viscous (no shear forces). The conservation equations of mass, momentum and energy for the capacitor and projectile shocks are, respectively,

$$\rho_{c_o} w_c = \rho_c (w_c - u_c)$$

$$P_{c_o} + \rho_{c_o} w_c^2 = P_c + \rho_c (w_c - u_c)^2 \tag{3}$$

$$e_{c_o} + \frac{P_{c_o}}{\rho_{c_o}} + \frac{w_c^2}{2} = e_c + \frac{P_c}{\rho_c} + \frac{(w_c - u_c)^2}{2}$$

and

$$\rho_{p_o} w_p = \rho_p (w_p - u_p)$$

$$P_{p_o} + \rho_{p_o} w_p^2 = P_p + \rho_p (w_p - u_p)^2 \tag{4}$$

$$e_{p_o} + \frac{P_{p_o}}{\rho_{p_o}} + \frac{w_p^2}{2} = e_p + \frac{P_p}{e_p} + \frac{(w_p - u_p)^2}{2} \ ,$$

where

ρ = density of material
w = shock velocity
u = particle velocity
P = pressure of material
e = internal energy of material.

The subscripts p and c refer to the compressed projectile and capacitor material, respectively. The subscripts p_o and c_o refer to the uncompressed projectile and capacitor material. Now Equations (3) and (4) can be combined to yield the normal relations for shock velocity, particle velocity, pressure and internal energy behind the capacitor shock,

$$w_c = \sqrt{\frac{\rho_c}{\rho_{c_o}}\left(\frac{P_c - P_{c_o}}{\rho_c - \rho_{c_o}}\right)}$$

$$u_c = \sqrt{\frac{\left(P_c - P_{c_o}\right)\left(\rho_c - \rho_{c_o}\right)}{\rho_c \rho_{c_o}}} \tag{5}$$

$$P_c - P_{c_o} = \rho_{c_o} w_B u_B$$

$$e_c - e_{c_o} = \frac{1}{2}\left(P_c + P_{c_o}\right)\left(\frac{1}{\rho_{c_o}} - \frac{1}{\rho_c}\right)$$

and behind the projectile shock

$$w_p = \sqrt{\frac{\rho_p\left(P_p - P_{p_o}\right)}{\rho_{p_o}\left(\rho_p - \rho_{p_o}\right)}}$$

$$u_p = \sqrt{\frac{\left(P_p - P_{p_o}\right)\left(\rho_p - \rho_{p_o}\right)}{\rho_p \rho_{p_o}}} \tag{6}$$

$$P_p - P_{p_o} = \rho_{p_o} u_p w_p$$

$$e_p - e_{p_o} = \frac{1}{2}\left(P_p + P_{p_o}\right)\left(\frac{1}{\rho_{p_o}} - \frac{1}{\rho_p}\right) .$$

Now for highly condensed media Stanyukovich[5] recommends a polytropic relation between pressure and density

$$P = \sigma\rho^{\gamma} ,$$

where γ is the polytropic exponent. From this relation the internal energy of a medium may be expressed as

$$e = \frac{1}{\gamma - 1}\frac{P}{\rho} . \tag{7}$$

Combining Equation (7) with Equation (5) yields for the capacitor

$$\frac{\rho_c}{\rho_{c_o}} = \frac{\dfrac{\gamma_c + 1}{\gamma_c - 1} - \dfrac{1}{P_c/P_{c_o}}}{\dfrac{\gamma_{c_o} + 1}{\gamma_{c_o} - 1} \Big/ \dfrac{P_c}{P_{c_o}} + 1} \tag{8}$$

and for the projectile

$$\frac{\rho_p}{\rho_{p_o}} = \frac{\dfrac{\gamma_p + 1}{\gamma_p - 1} - \dfrac{1}{P_p/P_{p_o}}}{\dfrac{\gamma_{p_o} + 1}{\gamma_{p_o} - 1} \Big/ \dfrac{P_p}{P_{p_o}} + 1} . \tag{9}$$

Now to render the problem tractable the assumption of strong shock wave theory $\left(\frac{P_c}{P_{c_o}}, \frac{P_p}{P_{p_o}} \gg 1\right)$ will be made in that the density ratio is assumed to reach a limiting value. While this is not strictly true, it provides a reasonable approximation and enables the derivation of simple expressions for the thermodynamic states generated on impact.[6] Thus using the strong shock approximation, the limiting density ratios for the capacitor and projectile,

$$\frac{\rho_c}{\rho_{c_o}} = \frac{\gamma_c + 1}{\gamma_c - 1} \tag{10}$$

$$\frac{\rho_p}{\rho_{p_o}} = \frac{\gamma_p + 1}{\gamma_p - 1} \quad , \tag{10}$$

are obtained from Equations (8) and (9).

When the strong solution for density, Equation (10), and the strong strong shock conditions $\left(\frac{P_c}{P_{c_o}}, \frac{P_p}{P_{p_o}} \gg 1\right)$ are employed along with Equations (1), (2), (5) and (6) it may be shown that the impact pressure in shocked states for the capacitor and projectile is given by the relation

$$P_c = P_p = \frac{\gamma_c + 1}{2} \rho_{c_o} \frac{v_o^2}{\left[1 + \sqrt{\frac{\gamma_c + 1}{\gamma_p + 1} \frac{\rho_{c_o}}{\rho_{c_o}}}\right]^2} \quad . \tag{11}$$

The temperature in shocked states can be obtained from the energy equations for the projectile and capacitor if the strong shock relations for pressure and density are used and the assumption is made that all the increase in internal energy goes to increase the temperature, or $e = c_v T$, where T = temperature of the media and c_v = constant volume heat capacity. Thus the temperature of the capacitor in the shocked states is

$$T_c - T_{c_o} = \frac{1}{2c_v} \frac{v_o^2}{\left[1 + \sqrt{\frac{\gamma_c + 1}{\gamma_p + 1} \frac{\rho_{c_o}}{\rho_{p_o}}}\right]^2} \quad . \tag{12}$$

The temperature of the projectile in shocked states is given by

$$T_p - T_{p_o} = \frac{1}{2c_v} \frac{\rho_{c_o}}{\rho_{p_o}} \frac{\gamma_c + 1}{\gamma_p + 1} \frac{v_o^2}{\left[1 + \sqrt{\frac{\gamma_c + 1}{\gamma_p + 1} \frac{\rho_{c_o}}{\rho_{p_o}}}\right]^2} \quad . \tag{13}$$

Hence with Equations (11), (12), and (13) the pressure and temperature of both the projectile and capacitor can be predicted following impact.

The pressure and temperatures of the impact states have been calculated for several projectile-capacitor front plate combinations and are presented in Figures 5, 6, and 7. In these calculations the value of the polytropic exponent relating the pressure and density of the highly

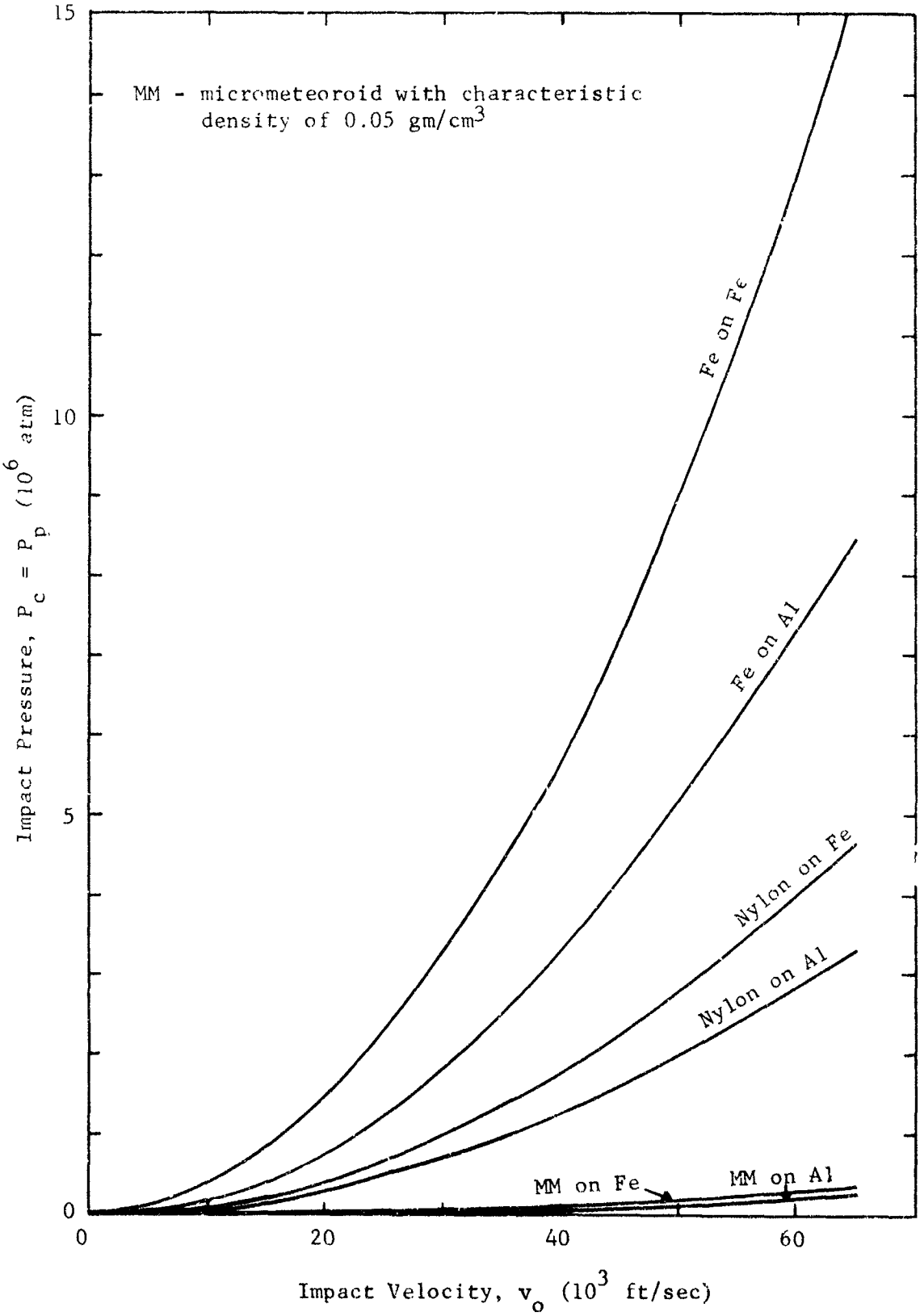

Figure 5. Initial interface pressures in one-dimensional impact

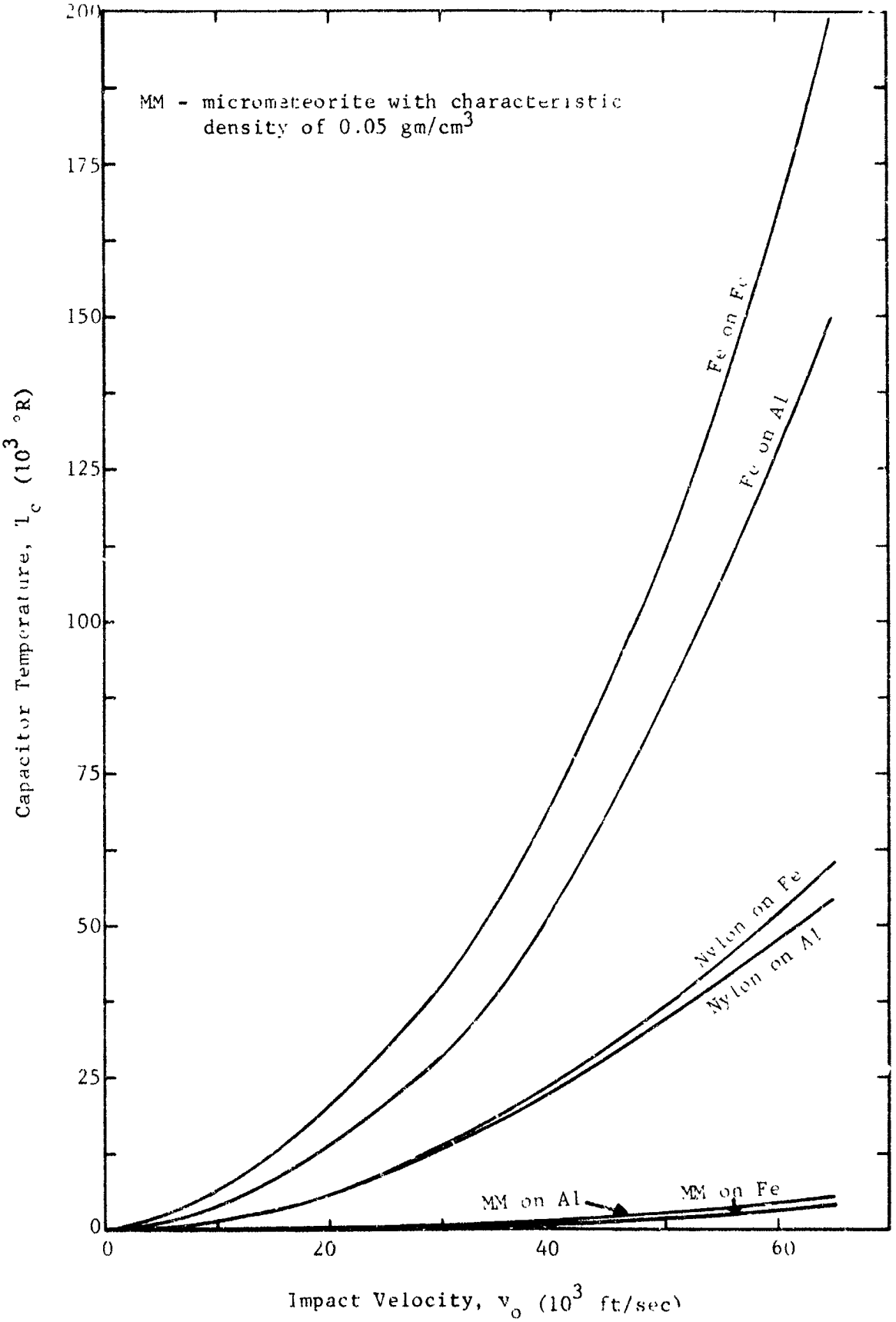

Figure 6. Initial capacitor temperature in one-dimensional impact

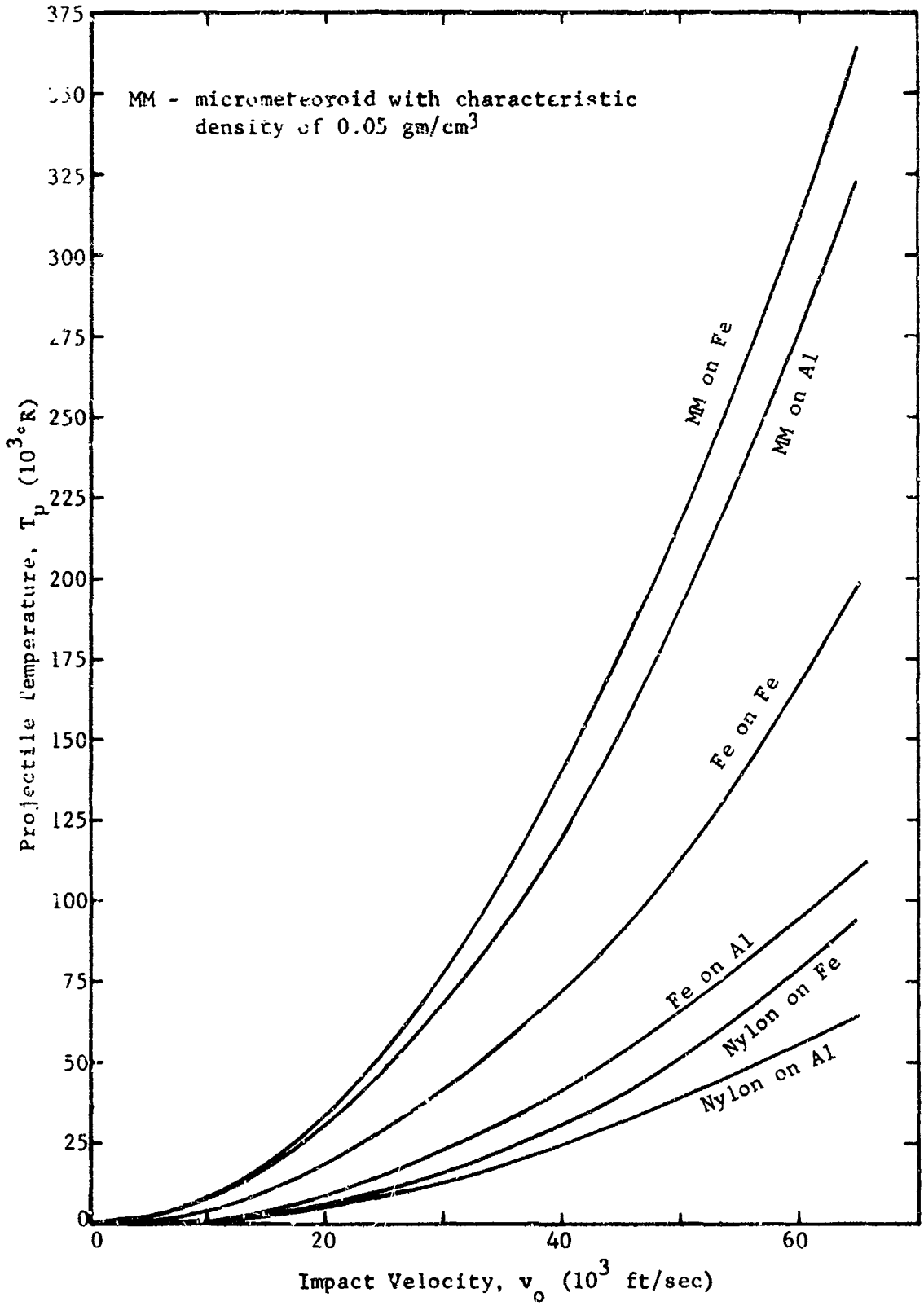

Figure 7. Initial projectile temperature in one-dimensional impact

condensed states encountered behind the impact shocks was taken as 3 which is a value currently thought to be most representative of the highly shocked impact states.[5] Also γ_p was taken equal to γ_c.

The impact pressures predicted in Figure 5 are felt to be representative of the actual impact pressures since they agree quite well with the impact pressures predicted by more laborious and exacting methods for solution of the mechanical shock relations where the actual Hugoniot properties of the shocked media are known.

The temperatures of the capacitor front plate and projectile predicted in Figures 6 and 7 appear to be satisfactory to a first approximation. However the effect of density change on the temperature change has been neglected and the energy absorbed due to the melting and ionization of the projectile and capacitor material which is known to occur in the initial stages of impact[7] have not been taken into account. Hence the extremely high temperatures at the higher velocities indicate the breakdown of the simple ideal gas expression $e = c_v T$ used to predict the temperatures in Figures 6 and 7. This may be explained by noting that when a strong shock wave occurs in a medium which is initially solid and the shock pressure is very high, that is of the order of 10^5 atmospheres, then although the atomic structure is destroyed by the high temperatures, the density is very high, so the material behaves more like a liquid with a very high vapor pressure than a gas. This liquid is highly ionized, so there are free electrons throughout. The higher atomic levels are split into bands because of the density and these bands may be only partially occupied as if the liquid were a metallic conductor. The electrons in these partially occupied bands behave very much like free electrons (the really free electrons have energies greater than the ionization potential). Thus the plasma produced by the shock acts like a fluid metal, being bound together by the free electrons in a lattice of positive ions, and hence exhibits considerable cohesion.

Plasmas, such as those mentioned above, have been observed with approximately 10^{19} free electrons per cm^3 and an average free electron lifetime of 10^{-8} to 10^{-7} sec at temperatures far below those required to ionize atoms and molecules thermally.[8] A typical conductance-trace[9] of this type plasma is shown in Figure 8. Due to the strong cohesion properties exhibited by these plasmas it appears that the formation of the plasma at relatively low temperatures is made possible by virtue of its existance in a quasi lattice. The lattice energy of this type plasma is formulated by assuming that the plasma lattice is similar to a metal lattice where the electrons are considered to form a rapidly circulating electron lattice in the much more slowly oscillating and more familiar positive-ion lattice. Based on this model Cook and McEwan[8] have formulated the total lattice energy which is given by the relation

$$- E = Z^2 B/d - 25\, Z^{2/3}/d^2 \text{ (ev)} \tag{14}$$

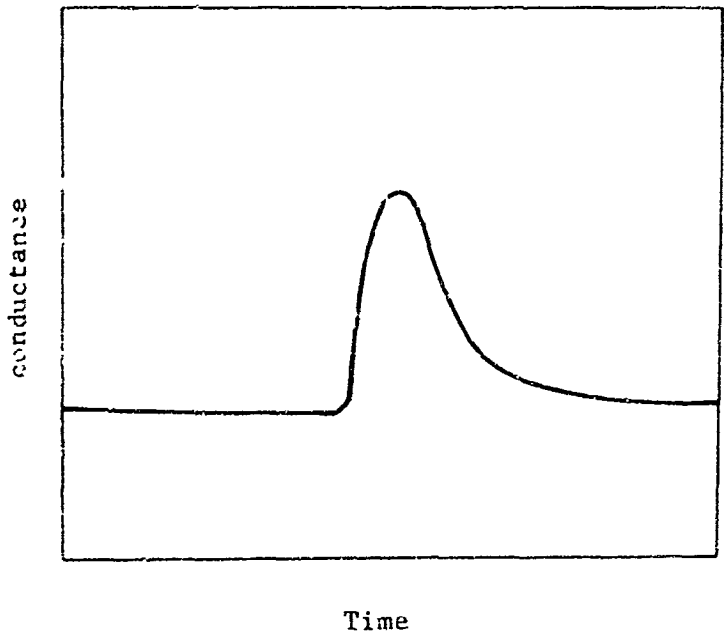

Figure 8. Typical conductance-time trace of a dense metal-like plasma[9]

where

Z = number of electrons per positive ion

d = the average ion-ion distance (Å)

B = an empirical constant

In this quasi-lattice model of the plasma the average lattice of cohesive energy will be approximately that given by the above equation with $B \approx 30$. This is true, however, only if $-E$ is larger than kT where T is the temperature of plasma. That is, a plasma of Z electrons per positive ion once formed will assume a quasi-lattice structure similar to the metal during the interval of its existance only if $|E| > kT$. This simply means that the effective ionization energy I_{eff} in a plasma of this type should therefore be given not by the ionization potential in a vacuum, $\sum_{i=1}^{Z} I_i$, but by

$$I_{eff} = \sum_{i=1}^{Z} I_i - |E| \quad .$$

Thus it is seen that it is possible for ionization to occur at much lower temperatures than normally required for thermal ionization of an atom or a molecule.

Cook[9] has also observed intense light emission in these highly compressed plasmas and has suggested that this light emission observed in the plasma is associated with the rapid electron circulation corresponding to radiation in non-quantum orbits. That is, the kinetic energy of the rapidly circulating electron lattice would cause the electrons to radiate because they circulate in non-quantum states. Thus the quasi-lattice model of these plasmas not only accounts for the formation of a plasma at much lower temperatures than normally required for thermal ionization but also accounts for the intense luminosity of the plasma. Apparently the luminosity of this type plasma along with the rarefaction waves R_p and R_c in Figure 3 account for the light flash which occurs on impact.

Experimental observations of ionization produced by the impact of high-velocity projectiles on thick and thin targets have been reported in the literature[7, 10, 11] but none of these investigations dealt with the type of plasma formed. However, Friichtenicht[10] observed that his experimental results for impact on an 800 Å thick gold foil were consistent with the hypothesis that after a projectile penetrates a thin metal target it is accompanied downstream by a dense plasma formed from the vaporized target and that this plasma finally explodes.

The lattice energy for plasma in iron of the type described above has been calculated for the first ionization stage and found to be $|E| = 7.86$ ev while the first stage ionization potential is 7.90 ev. Since a highly ionized state appears to be occuring in the shocked regions of a steel projectile and capacitor front plate upon impact, therefore $I_1 \simeq |E| + kT$, or the effective ionization potential is of the order kT, $I_{eff} \approx kT$, where T is the temperature in the shocked regions of the projectile and capacitor.

5. MECHANISM OF CAPACITOR DISCHARGE

From the previous discussion of impact of a high-velocity projectile on a capacitor-type micrometeoroid detector two mechanisms of capacitor discharge are suggested by the very high pressures and temperatures generated in the capacitor and projectile. These two mechanisms may be operating together or separately to make the capacitor discharge.

The first of these mechanisms is electro-mechanical breakdown of the mylar dielectric due to the very high pressure transmitted to it by the capacitor shock S_c. The electro-mechanical theory of dielectric breakdown may be described[7] by considering the capacitor as a plane slab with electrodes free to follow the dielectric material. When a voltage, V is applied to the capacitor, the dielectric is subjected to an electrical compressive stress $\frac{\epsilon}{2}\left(\frac{V}{d}\right)^2$, where ϵ is the dielectric constant. The initial thickness d_o is then reduced to an equilibrium thickness d and the electrical stress is balanced by an internal mechanical stress given by Hooke's law for large strains as $Y \ln d_o/d$ where Y is Young's modulus for the material. Therefore at equilibrium

$$\frac{\epsilon}{2}\left(\frac{V}{d}\right)^2 = Y \ln \frac{d_o}{d} \quad . \tag{15}$$

Now the compressive force increases with $1/d^2$ while the opposing force increases only as $\ln d_c/d$. The product $d^2 \ln d_o/d$ has a maximum (with respect to d) when $d/d_o = 0.6$ and no stable thickness exists for $d < 0.6\ d_o$. Although the intrinsic breakdown strength has not been reached, failure occurs due to mechanical collapse, and the breakdown strength of the dielectric is given by Equation (15) with $d = 0.6\ d_o$ or

$$E_B = \left[\frac{2Y}{\epsilon} \ln \frac{10}{6}\right]^{1/2} \quad .$$

Consider a similar capacitor structure with an applied voltage V across it and a mechanical pressure applied to it at a localized area on the face of one of the electrodes. The applied mechanical pressure required to cause electro-mechanical breakdown under these conditions has been determined and is given by the realtion

$$P_{appl} = \frac{\epsilon E_B^2}{2}\left[1.95\ (\ln E_B - \ln \frac{V}{d_o}) - 1\right] \cdot$$

This equation is plotted in Figure 9 for voltages ranging up to 150 v applied across a capacitor with a 1/4 mil Mylar dielectric with a breakdown strength of 10^8 v/m and a relative dielectric constant of 3. It is seen from this figure that an applied stress of 1500 atms would

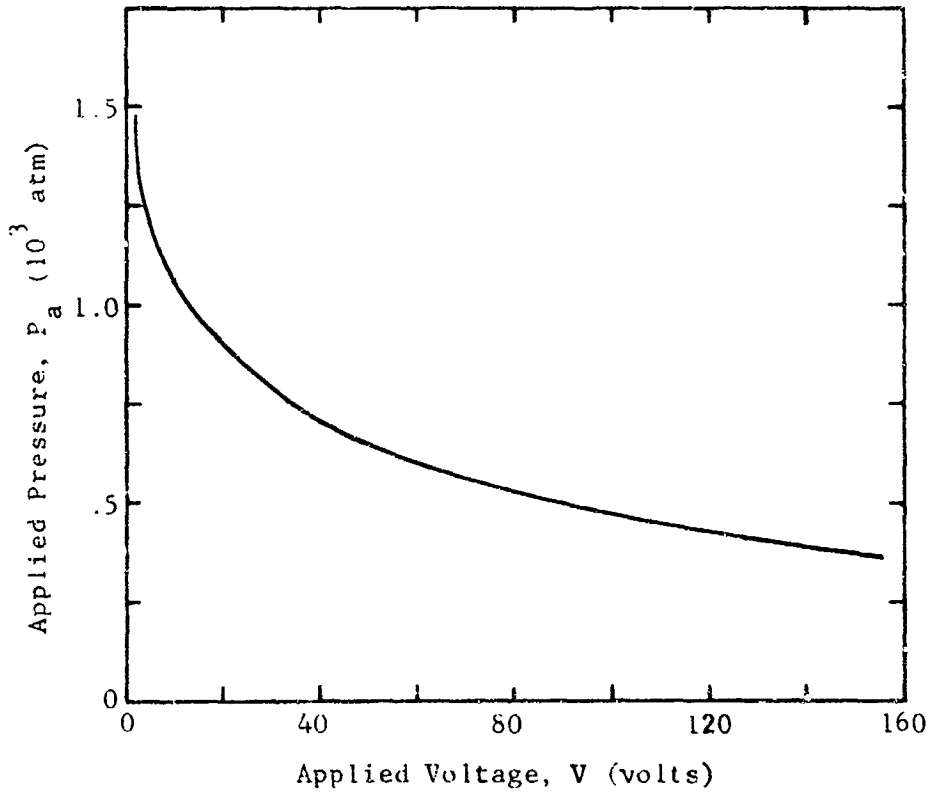

Figure 9. Static pressure P_a required to initiate elector-mechanical breakdown of 0.25 mil Mylar dielectric capacitor with applied voltage V

be enough to break down the dielectric and cause the capacitor to discharge. Assuming that the shock-induced impact pressure is completely transmitted to the Mylar dielectric and that this dynamic pressure is approximately equivalent to a static applied stress the pressure required to break down the Mylar is, from Figure 5, obtained at impact velocities of 1000 ft/sec, 2000 ft/sec, and 5000 ft/sec for steel, nylon and micrometeorite projectiles impacting the capacitor. Thus, from Figure 5, the pressure required to initiate the electromechanical breakdown mechanism is obviously available at all but the lowest impact velocities. However, this pressure-induced breakdown mechanism does not give an explanation for sustaining the capacitor discharge. To do this a second mechanism of capacitor discharge must be invoked. Thus for a sustained capacitor discharge the second mechanism must be occurring and the pressure-induced mechanism may occur. This can be seen by a simple electrical analog which describes the discharge and recharge transients. To simplify the calculations the resistance of the breakdown paths between the electrodes of the capacitor will be assumed to be constant for a time $0 \leq t \leq \tau$ and then increase to infinity in negligible time for $t > \tau$. The equivalent circuit at time $t = 0+$ after initiation of breakdown is shown in Figure 10. Analysis of this circuit yields a value of voltage across R_L equal to

$$v_{RL} = \frac{R_L V_c}{R_L + R_B}\left(e^{\frac{-t(R_L + R_B)}{R_L R_B C}} - 1\right) \quad 0 \leq t \leq \tau \tag{16}$$

and for the condition $R_B \ll R_L$ reduces to

$$v_{RL} \simeq V_c \left(e^{\frac{-t}{R_B C}} - 1\right) \quad . \tag{17}$$

From Equation (17) the voltage across the load resistor R_L at time $t = \tau$ is

$$v_{R_L}(\tau) = V_d \simeq V_c \left(e^{-\tau/R_B C} - 1\right) \tag{18}$$

and has been identified as the discharge voltage V_d. The recharge transient across the load resistor R_L is

$$v_{RL}(t) = (V_c - V_d)\, e^{\frac{-t}{R_L C}} \qquad \tau < t \quad . \tag{19}$$

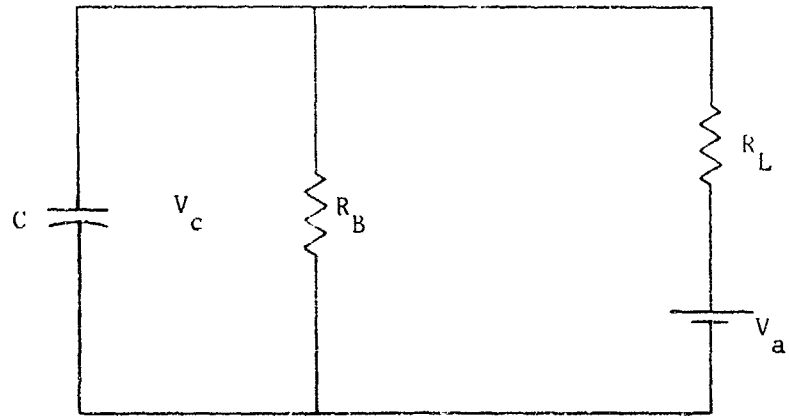

Figure 10. Equivalent circuit for capacitor discharge due to micrometeoroid impact where it is explicitly assumed that $V_c = V_a$ at time $t = 0$ and R_B is the discharge resistance through the capacitor

For this simple model we have identified R_B with the minimum value of resistance between the electrodes of the capacitor during the breakdown pulse. To observe approximately full discharge $V_d \simeq V_c$ the discharge must be sustained for a time $\tau > 3\ R_B C$. For the various observations reported by NASA, a mechanism which results in a correlation between the conductivity and lifetime of the breakdown can be postulated. This second mechanism of capacitor discharge is related to the large quantities of thermal energy available in the highly shocked regions of the capacitor and projectile immediately following impact. This thermal energy is sufficient to generate in this region a highly compressed plasma of the type previously discussed. This highly-conducting dense plasma material in the shocked regions of the projectile and the capacitor front plate penetrates through the capacitor structure at some particle velocity u_c' and sets up a conduction path between the front and back electrode for a short period of time. The capacitor discharges a portion of its stored charge through the low resistance path. The magnitude of the discharge voltage will depend on the conductivity and lifetime of the plasma. As the plasma passes through the capacitor structure some of it probably will be left on the internal surfaces of its path of penetration. After a short time this material will drop out of the plasma state and then be vaporized by the transient current. Thus, in this second mechanism, the capacitor discharge is initiated and sustained by a dense plasma which is generated on impact and penetrates through the capacitor, momentarily producing a low but finite resistance path between the electrodes.

Another aspect of the detection of micrometeoroids by capacitor discharge is the transmission of the signal from the point of penetration to the detection circuits. For a large area capacitor, the transmission path from the impact site to the boundary may be treated as a transmission line as described in Appendix C. As a result of this idealized analysis, it is apparent that significant signal energy can be dissipated in the transmission path. For the geometry of the capacitor detector considered in this analysis with an electrode area of approximately 4 in^2 the maximum signal energy loss in the transmission path for a 20μ diameter penetration radius is approximately 6db and for a 200μ diameter is approximately 3 db. For penetrations near the boundary the energy loss decreases. If the penetrations are at random over the area of the detector the average value of energy loss in the transmission path resulting from a number of impacts is less than 3 db. One can decrease this loss by increasing the thickness of the thinnest aluminum electrode.

This analysis assumes that a lossless transmission line is matched to the boundary of the capacitor and terminated at the detection circuits. If these requirements are not met, transients characteristic of signal transmission such as ringing may result. From this brief analysis, it is evident that careful consideration should be given to the geometry of the capacitor electrodes and to the method of signal transmission from the capacitor to the detection circuits. The above analysis is somewhat pessimistic in that signal power loss has been considered while

the detection circuits respond to pulse height. Therefore the 3 db loss value represents a pulse at the boundary of the capacitor which is .707 of the height of the true discharge pulse. As indicated in Appendix C the character of the pulse has been altered by the increasing loss with increasing frequency. This results in an increase in the rise time of the pulse. Since the frequency response of the equivalent transmission line decreases by less than a factor of 2 from 1 cps to 10^5 cps, the rise time considerations are of secondary importance for this particular analysis.

6. CORRELATION OF EXPERIMENTAL OBSERVATIONS WITH THE THEORETICAL MODEL

If the impact model discussed in section 4 is correct, then it should be possible to correlate the majority of the experimental observations discussed in section 3 with this model. This is done for the more significant of the experimental observations.

The experiments of Lewis Research Center indicated that for tests conducted in a vacuum the magnitude of V_d was found to be 10 to 15% higher than for tests conducted in ambient air. This is explained by the effect of the electron affinity of air on the plasma conductivity. Now free electrons contirubte practically the entire conductivity of the dense plasmas. Conduction measurements in these dense plasmas by Cook, Keyes, and Eudy[12] have shown that the electron affinity of the gaseous ambient is important in determining their conduction characteristics. Of the gaseous ambients studied conduction in the plasma decreased as the effective electron-affinity of the ambient medium increased. This is because generation of free electrons in the plasma is retarded by the high electron-affinity of the ambient medium.

The experimental results of Lewis Research Center also indicated that a positive polarity on the outside aluminum electrode, and a negative ground on the steel plate of the coincidence type capacitor enhanced the discharge mechanism. This is consistent with the experimental observations of Cook, et al.[12] in that there is an appreciable drop both in the velocity and conduction in a dense plasma when it propagates into an electric field which is parallel and opposite to the mean velocity vector of the plasma.

Bill Kinard of Langley Research Center reported that when 0.22 caliber Nylon cylinders were fired at the first thin film capacitor discussed in section 3 the capacitor did not discharge but when the capacitor was backed by a bakelite plate it did. This is explained by the fact that when a projectile impacts a thin target where the ratio of the target thickness to the projectile diameter is very small the compression shock propagated in the capacitor structure reflects from the back free surface as a rarefraction wave and this rarefraction wave destroys the shock-induced conditions in the capacitor almost immediately. Since the transfer of thermal energy is slower than the transfer of momentum the rarefraction wave quenches the ionization process in the capacitor and the projectile before it has time to develop. However when the capacitor is backed by a bakelite plate the shock wave incident on the bakelite reflects as a compression shock and hence the shock-induced conditions in the projectile and capacitor are not cancelled and the ionization process occurs.

It was also noted from these experiments that the discharge pulse amplitude depended on the velocity of the penetrating particle and that $V_d \longrightarrow V_c$ for velocities in the range of 10^4 ft/sec. For the velocities below this limiting value the discharge voltage ranged over 3 to 4 orders of magnitude as the velocity of the particle was increased.

This observation is explained from the impact model and the plasma mechanism of discharge. The conductivity of the plasma will be governed by its degree of ionization which is determined by the thermal energy available for ionization in the shocked regions of the capacitor and projectile. The amount of thermal energy available is obviously a function of impact velocity as seen from Figures 6 and 7. The fact that $V_d \longrightarrow V_c$ for velocities in the range of 10^4 ft/sec for $V_c \approx 15$ volts is explained by the fact that velocity and hence the energy available for ionization is sufficient to ionize the dense plasma to the point where its conductivity is large enough to completely discharge the capacitor within the limits of the external circuitry. The fact that the signal level covers three to four orders of magnitude as the impact velocity is increased may be due to pressure induced breakdown occurring at the lower velocities without ionization being produced to sustain the capacitor discharge.

It was also reported in the Langley experiments that spectral measurements taken during the impact indicated that there was ionization of the projectile and capacitor front plate. This is explained by the fact that highly-ionized material is ejected rearward from the internal shock regions by the formation of rarefraction waves R_p and R_c as seen in Figure 3.

Tests were also conducted by Langley on a similar capacitor structure but with a thicker (1 mil) front aluminum electrode. It was observed that the capacitor was more likely to discharge when penetrated in ambient air than in a vacuum. This may be explained by noting that when the capacitor is penetrated in air it is possible for a discharge to occur even though a dense metal plasma is not formed. The discharge occurs because a conduction path is set up between the electrodes due to the ionized air trail left by the projectile as it penetrates the capacitor.

For this thicker capacitor the value of V_d ranged from 0 to V_c but with a bakelite backup plate V_d equalled V_c. The explanation for this is the same as for the case where a bakelite plate was used for the first and thinner capacitor. The reason that a discharge may be observed in this thicker capacitor structure is that because of the increased thickness it takes longer for the release rarefraction wave to get back to the primary shock region of the projectile and capacitor and hence the ionization process has time to occur.

Experimental observations of the light flash indicate that the major portion of the light seemed to emanate from the incident surface with only a minor flare at the exit hole. The explanation for the light flash is that the formation of rarefraction waves R_p and R_c in Figure 3 results in the rearward ejection of the highly-luminous plasma material existing in the shocked regions of the capacitor and projectile. The light flash is less intense on the downstream side of the capacitor because as the dense plasma passes through the capacitor structure, it expands and recombination begins. Thus when this material exits from the back of the capacitor it is not as highly ionized as it was immediately

after impact and hence its luminosity has decreased considerably. It has also been observed that the duration of the light flash correlates with the bottoming of the discharge pulse. This is because the light emission of the dense plasmas is a result of the same mechanism that causes conduction in these plasmas. Cook, et al.,[12] have observed experimentally that the conduction zone of these plasmas corresponds precisely to the luminosity zone. This supports the concept that the luminosity, like the conduction, is related to the concentration of free electrons.

Jim Siviter of Langley Research Center reported that in tests conducted on a thin aluminum-plate capacitor the discharge voltage was proportional to the magnitude of the applied voltage. This observation is explained by Equation (18). It was also pointed out that the two distinctly different types of pulses were observed on discharge. One was a nice clean pulse with a sharp peak while the other had multiple peaks for a certain length of time and then decayed. It is possible that both types of pulses may be due to ionization-initiated discharge. The same type of unstable behavior seen in the second pulse has been observed in dense plasmas. Bauer, et al.,[13] observed experimentally that when a dense plasma was over-compressed, on subsequent expansion it over-expands past its equilibrium point and becomes unstable as recombination occurs and finally explodes. This behavior is readily explained by the quasi-lattice model of dense plasmas. Apparently this type of plasma has a characteristic density and when the plasma is compressed to a higher density and released it expands like a spring beyond its equilibrium density where it explodes. This is because the stability falls off when the density decreases as explained by the quasi-lattice model. This explanation is correlated to the impact model in that the dense plasma formed initially at impact will begin to expand as it passes through the capacitor structure and hence the unstable behavior described above might be expected to occur.

Tests were also conducted on a similar capacitor structure but with a stainless steel electrode and it was observed that the discharge signal was 15% larger than for the previous capacitor structure with the aluminum electrode. This is due to the fact that the amount of thermal energy available for ionization in the shock zone of the capacitor and projectile is greater for impact on steel than impact on aluminum as seen in Figures 6 and 7. Thus the steel is more highly-ionized than the aluminum, the conductivity of the dense plasma is greater, and the discharge voltage is larger.

J. Broderick of Langley reported on tests conducted at North American Aviation on a capacitor with a 1 mil stainless steel front electrode. It was found that the average discharge voltage was proportional to the applied voltage. This observation is explained by Equation (18). It was also noted that when tests were conducted on a similar capacitor with an aluminum front electrode the light flash was less intense than for a stainless steel electrode. This is because the luminosity of these dense plasmas is, like the conductivity, proportional to the concentration of free electrons and thus if a lower discharge

voltage is observed for impact on an aluminum electrode than for a stainless steel electrode, as it was, then the luminosity would be less intense.

Broderick also reported that there was a more intense impact light flash when a lower applied voltage was across the capacitor. This occurs because the polarity of the capacitor was such that the applied electric field was parallel and opposite to the direction of plasma propagation. Therefore the conductivity, and hence the luminosity of the dense plasma would then decrease as the applied electric field was increased. As mentioned in the previous paragraph it was also observed that under similar polarity conditions the discharge voltage increased as the applied voltage was increased. At first glance this observation may be questioned because the conductivity of the dense plasma is known to decrease for an increasing electric field of this polarity. However the plasma propagation velocity also decreases for similar electric field conditions and a higher resistance conduction path R_B would remain across the capacitor electrodes for a longer period of time τ. Thus if τ/R_B in Equation (18) changes in such a manner that $V_c e^{-\frac{\tau}{R_B C}}$ increases faster than V_c, as V_c is increased then the discharge voltage V_d would be expected to increase.

7. AMBIGUOUS SIGNAL GENERATION

To function as a micrometeoroid detector the electrical pulses which can register a count in the detection circuits must originate from the phenomena associated with impact. Presently, there are data obtained from experiments conducted by NASA which indicate that other aspects of the space environment can lead to ambiguous signals. At Langley Research Center aluminum-Mylar-aluminum capacitor type micrometeoroid detectors were irradiated in a Van den Graff accelerator with electrons incident on the 1 mil of aluminum as shown in Figure 11. The energy of the electrons was varied between 20 and 150 kev at a flux rate of 10^9 to 10^{11} e/cm^2-sec and a total dose of 10^{13} to 10^{14} e/cm^2. In one series of experiments, voltage pulses were obtained from the capacitor over the entire energy range of the incident electrons with the maximum number of pulses in a total dose of 3.25×10^{13} e/cm^2 occurring at approximately 30 kev. Also it was noted that the number of pulses decreases with increasing temperature but that dose rate (total dose held constant) and the applied voltage have little effect upon the number of pulses. Pulses were obtained without a bias applied. The amplitudes of the observed pulses were primarily between 100 and 300 volts with only 15 volts across the capacitor.

A later experiment reproducing the electron energies, dose rates and total dose did not yield pulses for the structure shown in Figure 12. The capacitor was similar to the unit used in the previous experiments. However there was no back-up plate and the 1 mil aluminum was grounded. If the detector was backed by a thick piece of metal, pulses were obtained in the 150 - 200 kev range with a pulse about every 5×10^{14} e/cm^2. Removal of the back-up plate eliminated these pulses.

A series of experiments have been performed at Ling-Temco-Vought under the direction of Marshall Space Flight Center. The energy of the electrons was varied from 550 - 950 kev in 50 kev intervals. A bias voltage of 0 - 100 volts was applied to the structure shown in Figure 13. With an electron flux of approximately 10^{11} e/cm^2-sec and a total flux ranging from approximately 10^{14} e/cm^2 to 2×10^{15} e/cm^2, pulsing of the detector was observed. At 650 kev the number of pulses for the total flux used in irradiating each detector yielded an averaged ratio of flux per pulse of 4.6×10^{12} e/cm^2.

Although these data are incomplete and do not lead to an obvious conclusion as to the cause of the pulses upon irradiating the detector, these observations do indicate that the effects of a radiation environment upon the operational characteristics should be fully investigated through analysis and space simulation experiments. To analyze the behavior of the detector in a radiation environment, one must consider the primary radiation and all secondary processes accompanying the slowing down and possibly stopping of the incident particle and the effect of these mechanisms upon the electrical properties of the materials used to construct the detector. Since the problem does not lend itself to an analytical solution based upon existing theories, a phenomenological description of the pertinent mechanisms will be included.

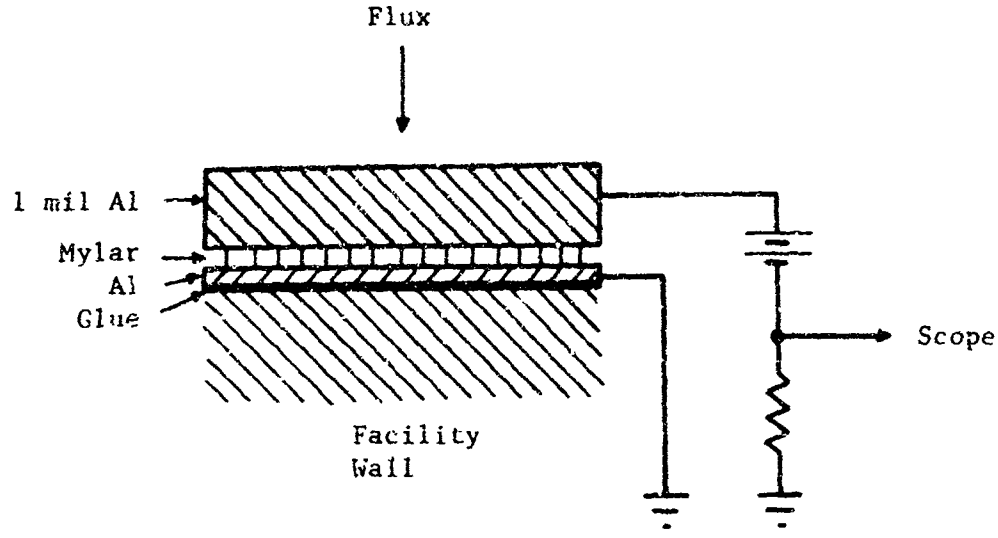

Figure 11. Arrangement of capacitor for electron radiation with evaporated aluminum electrode grounded

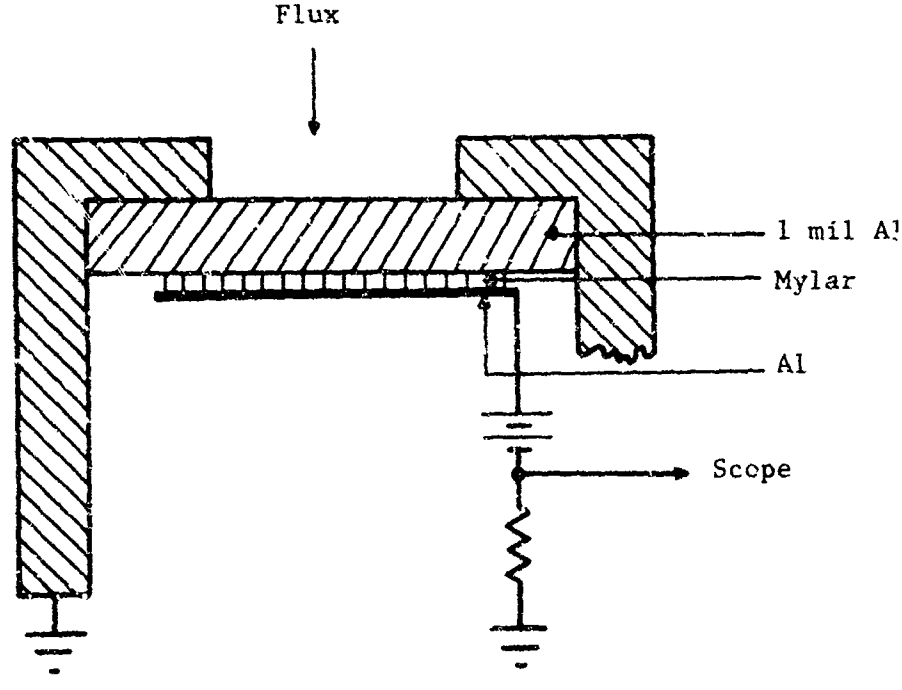

Figure 12. Arrangement of capacitor for electron radiation with 1 mil aluminum grounded

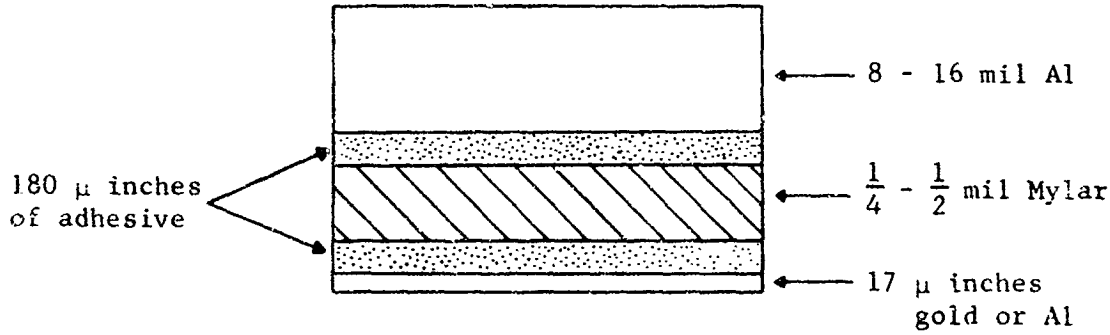

Figure 13. Capacitor type micrometeoroid detector tested at Ling Temco Vought

8. ELECTRON PENETRATION OF ALUMINUM

An electron incident on an aluminum electrode loses energy through ionization and bremsstrahlung. For moderate energy electrons radiative losses are small compared with ionization losses. The fraction of the incident electron kinetic energy (E in Mev) converted into bremsstrahlung in a thick aluminum target is approximately

$$\eta \simeq 9.1 \times 10^{-3} E \quad ; \tag{20}$$

the total bremsstrahlung energy I, in Mev per incident electron, is

$$I = 9.1 \times 10^{-3} E^2 \quad . \tag{21}$$

The photon spectrum created by incident electrons with an energy less than 50 kev can be approximated by the method shown in Figure 14, where the absorber has been divided into increments of thickness representing thin targets. For this situation it has been shown that

$$\frac{dI}{d\nu} = k_1 \, z(\nu_{max} - \nu) \quad , \tag{22}$$

where $h\nu_{max}$ corresponds to the electron energy E. However this does not describe the spatial distribution for the bremsstrahlung in traversing any remaining portion of the absorber. Over the energy range of interest photons interact with matter primarily by Compton scattering and the photoelectric effect. These interactions of electromagnetic radiation passing through matter are described qualitatively by attenuation coefficients for each method of interaction. Using a total linear attenuation coefficient μ_o a collimated beam of photons of initial intensity I_o yields, after traversing a thickness x of the absorber, a beam of unaffected primary photons equal to

$$I = I_o e^{-\mu_o x} \quad . \tag{23}$$

The attenuation coefficients for photons in aluminum are shown in Figure 15.

The loss of energy in a solid by bombarding electrons results in a transfer of energy to the electrons of the solid. This energy transfer is accomplished through a multiplicity of events where ionization and photo electrons diffuse the energy and momentum of the original beam. These cascade processes preclude exact analysis. However, secondary electron emission has been intensively investigated. Fortunately

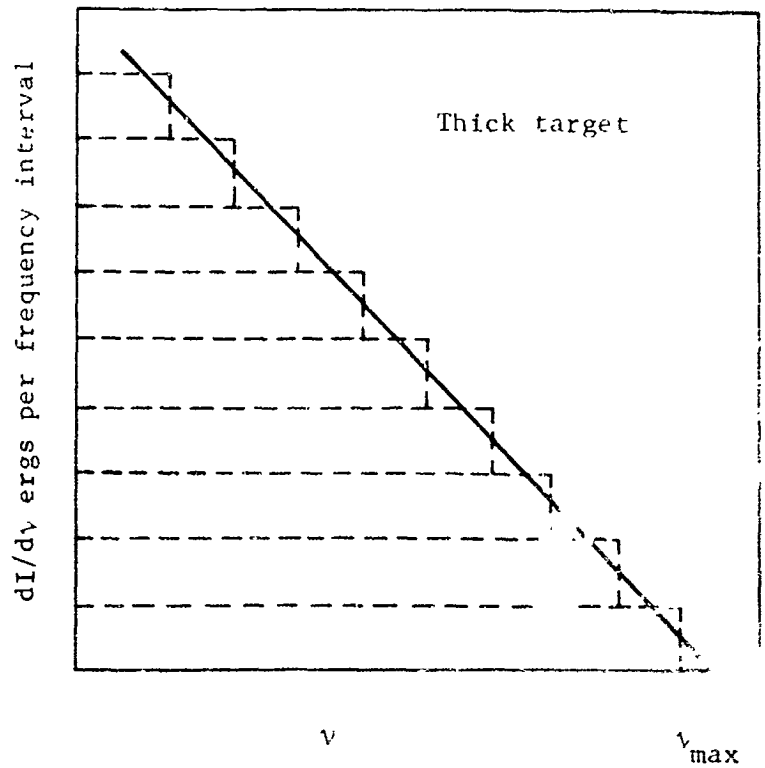

Figure 14. The bremsstrahlung intensity per frequency interval from a thick target[14]

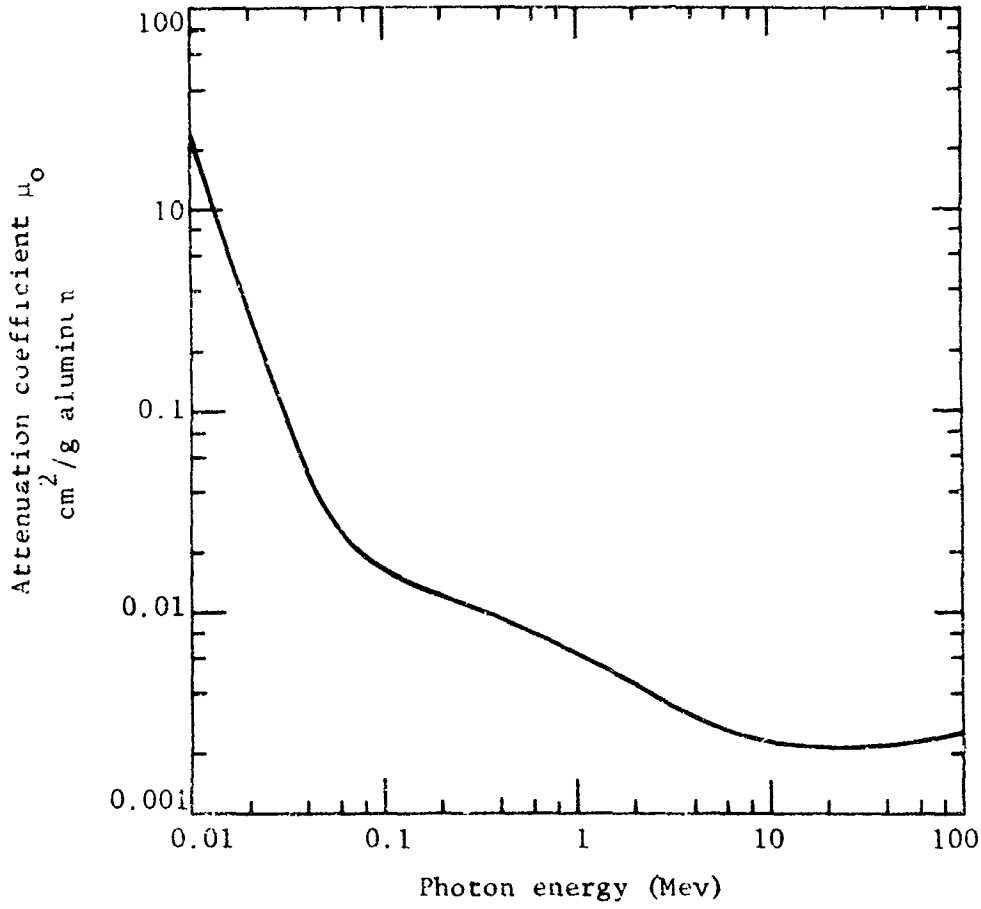

Figure 15. Mass attenuation coefficients for photons in aluminum[14]

for this analysis only the secondary electrons which are emitted are of interest. In particular the electrons which cross the boundary between the aluminum and Mylar must be characterized. Figure 16 shows an energy spectrum for the secondary electrons determined experimentally. The ratio δ of secondary electrons to primary electrons is shown in Figure 17 as a function of primary electron energy for two thicknesses of aluminum. The results indicate that the yield of secondary electrons with sufficient energy to be emitted from an aluminum surface increases as the energy of the primary electron beam dissipated within the aluminum target increases. For these data the primary electrons are energetic enough so that most of them are able to penetrate the target. For lower primary energies the secondary electron emission from the back surface of the target is expected to reach a maximum and then decrease as the primary electron energy is decreased. However a quantitative description of the processes involved would be extremely complex and experimental data which is directly applicable to the problem are not available. However from this series of experiments it is evident that a significant number of low energy secondary electrons enter the Mylar for primary energies from 1 Mev down to 200 kev and possibly lower.

It is also important to determine the number of primary electrons which penetrate an aluminum absorber. The range-energy relationship for electrons in an aluminum abosrber has been investigated extensively. Due to straggling there is no absolute range. Therefore an extrapolated range known as the practical range is usually chosen as a guide to the range of a monoenergetic beam of electrons. Some authors have described this range as the thickness of absorber required to reduce the intensity of the beam to a small portion (approximately 10^{-4}) of the incident beam intensity.[16] An empirical relationship which describes the range-energy values of interest to this discussion is

$$R_o = 412 \left(\frac{E}{Mev}\right)^n \frac{mg}{cm^2} \tag{24}$$

where $n = 1.265 - 0.0954 \ln\left(\frac{E}{Mev}\right)$.[21] This relationship is shown in Figure 18. One mil aluminum (6.86 mg/cm^2) corresponds to the practical range for 70 kev electrons. For approximate computations of the absorption of electrons one can assume that over a limited region the intensity of the beam varies exponentially with the abosrber thickness,

$$I = I_o \exp\left[-\frac{\mu x}{\rho}\right] \tag{25}$$

where $\frac{\mu}{\rho}$ is an apparent abosrption coefficient expressed in $\frac{cm^2}{mg}$ and x is the absorber thickness in $\frac{mg}{cm^2}$. A value of μ/ρ has been given as

$$\mu/\rho = \frac{22}{E_o^{1.33}} \tag{26}$$

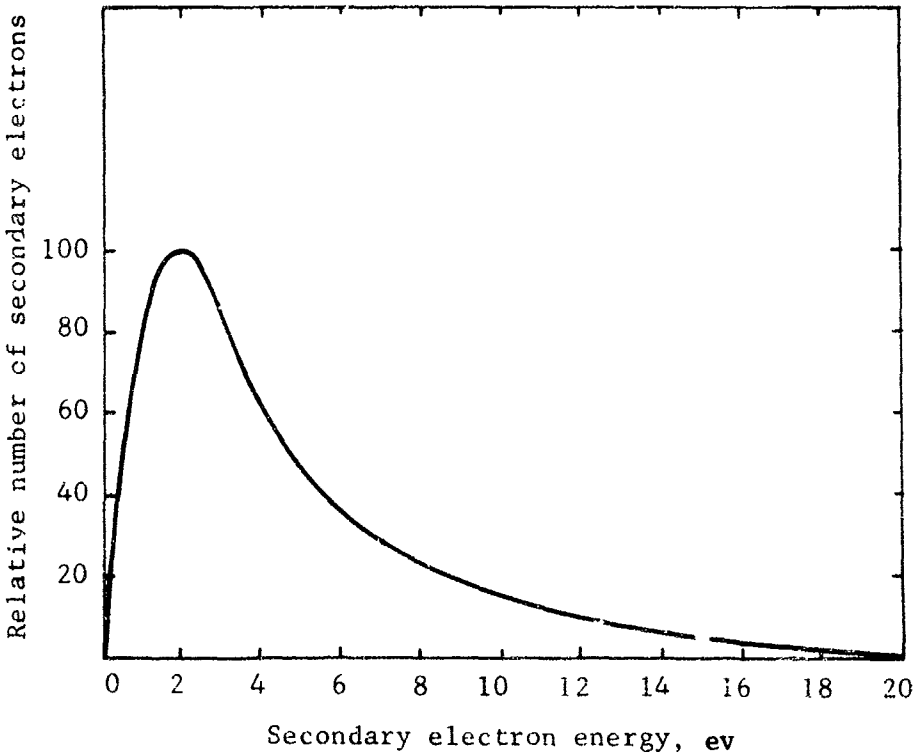

Figure 16. Energy spectrum of secondary electrons for aluminum[15] resulting from a primary beam of energetic electrons

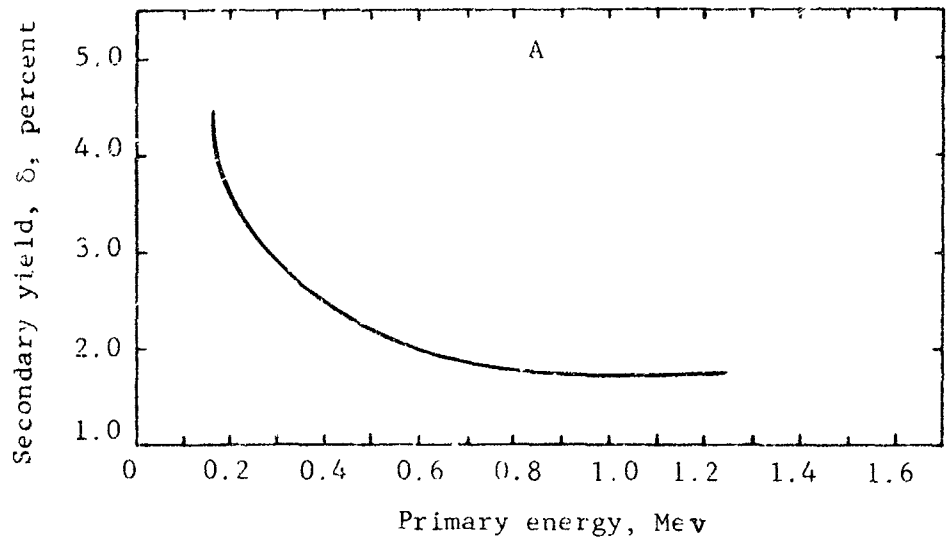

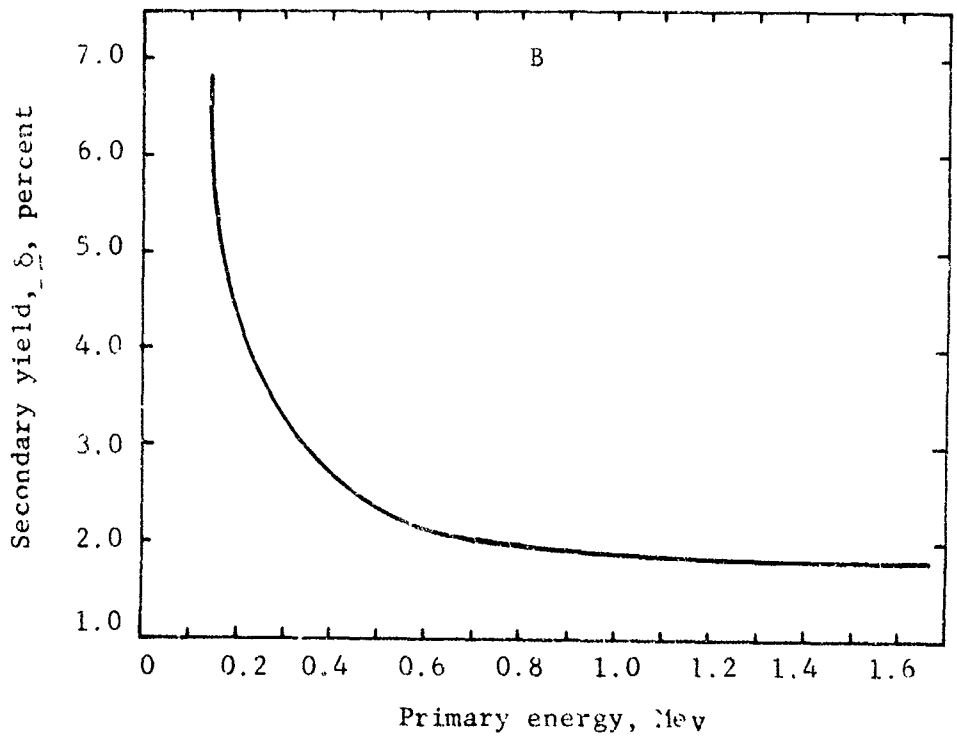

Figure 17. Yield vs energy data obtained with 1.8 mg/cm^2 (A) and 5.2 mg/cm^2 (B) Al target electrodes [15]

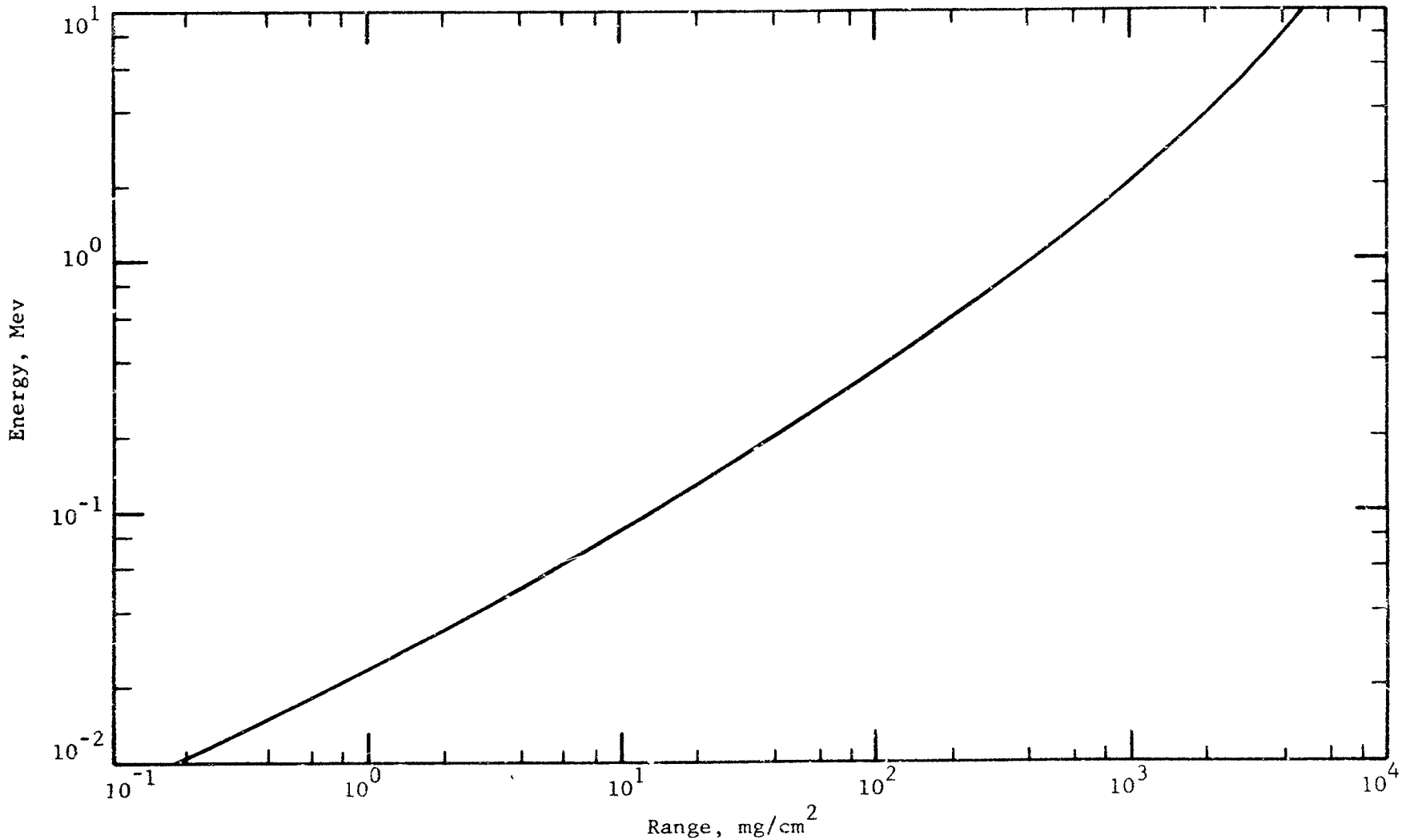

Figure 18. Range energy for monoenergetic electrons in aluminum[16]

for energies between 0.1 and 3.0 Mev.[16] An extension of these relationships can at best offer a crude approximation. For this analysis, these approximations can be used to indicate expected results. Thus if 70 kev monoenergetic electrons are incident on one mil aluminum with an integrated dose of 10^{14} electrons/cm^2, only 10^{10} electrons/cm^2 would pass through the aluminum. For 30 kev monoenergetic electrons approximately 10^7 electrons/cm^2 would pass through with the same integrated dose. For 200 kev electrons approximately 60% of the incident electrons will pass through.

From this analysis one obtains only approximations as to the number of electrons which penetrate the abosrber. An equally important consideration is the energy spectrum of the primary electrons after passing through the absorber. Little data that are specifically related to thick absorbers are available. However, under certain conditions the theories developed by Williams,[17] by Landau,[18] and by Bluck and Leisegang[19] can be used to approximate the energy distribution. The most probable loss is

$$\Delta E_p = W_1 \left\{ \log \frac{mv_1 W_1}{I^2 (1 - \beta^2)} - \beta^2 - K \right\} \quad \text{(Gaussian Units)} \qquad (27)$$

where

$$W_1 = 2\pi e^4 \frac{NZX}{mv^2} \quad .$$

And

e = charge of the electron
N = atoms/cm^3 for the abosrber
Z = atomic number for the absorber
X = thickness for the absorber
m = mass of the electron
v = velocity of the electron
β = v/c
I = average excitation potential energy in the absorber
K = 0.37 by Landau.

The full width (FWHM) at half-maximum for the straggling distribution is

$$\Gamma = 3.98\ W_1 \quad . \qquad (28)$$

From these equations it is possible to show that for a given thickness of aluminum, the most probable energy loss and the FWHM increase with a decrease in the energy of electrons. These relationships hold where scattering can be neglected and the cross section for a given energy

loss in a single encounter is independent of the variation in energy of the electron as it passes through the foil. The departure from this model for aluminum thicknesses where these assumptions do not hold indicates that there are more low energy electrons than one would predict.

For a one mil aluminum electrode and ¼ mil Mylar dielectric, values of most probable energy loss and FWHM can be obtained disregarding the model and recognizing the fact that the distribution will contain more low energy electrons than one would predict from the model. The calculated values of most probable energy loss for 1 mil aluminum and ¼ mil Mylar are shown in Figure 19. The calculated values of most probable energy of the primary electrons which penetrate the aluminum and enter the Mylar along with the FWHM of the energy distribution are shown in Figure 20. An illustration of the spectrum of the primary electrons that enter the Mylar through the aluminum is shown in Figure 21. These data are for beryllium which is a low Z element and would present a smaller cross-section to scattering than Al, however it is expected that aluminum would give similar data.

From these phenomenological discussions certain attributes of the interaction of electrons with a 1 mil aluminum target are apparent. For primary electrons with energies ranging from 200 to 600 kev, low energy secondary electrons are emitted from the aluminum surface with a yield ranging from approximately 10% to 1%. If the energy dissipated in the aluminum by the primary electrons increases, the yield increases. Over this energy range most of the primary electrons penetrate the aluminum.

As the energy of the primary electrons is decreased below 200 kev one can at best theorize about the primary and secondary electron emission at the back surface of the aluminum. Somewhere between 200 kev and 70 kev, where 1 mil aluminum corresponds to the practical range, one would expect the secondary electron yield to reach a maximum value. At the maximum secondary electron yield it is likely that the number of secondaries leaving the aluminum surface exceeds the number of primaries which penetrate the aluminum.

For the energies considered thus far the primary source of low energy electrons at the aluminum surface is multiple collisions which causes secondary electrons and straggling of the primaries. As the energy is decreased below 70 kev this may no longer be true. For example 30 kev electrons have a practical range of approximately 0.2 mils in aluminum. Therefore most of the primaries have dissipated their energy through ionizations and bremsstrahlung in the first 1/4 mil. The energetic secondary electrons whose energy is less than the primary energy will not have enough energy to reach the back surface of the aluminum. However the bremsstrahlung resulting from the slowing down of the primary electrons will pass through the aluminum and be attenuated in intensi by the creation of photo electrons. Although the fraction of the incident energy converted into bremsstrahlung is small ($\approx 0.03\%$), the total bremsstrahlung energy for a total dose of 10^{13} e/cm^2 at 30 kev

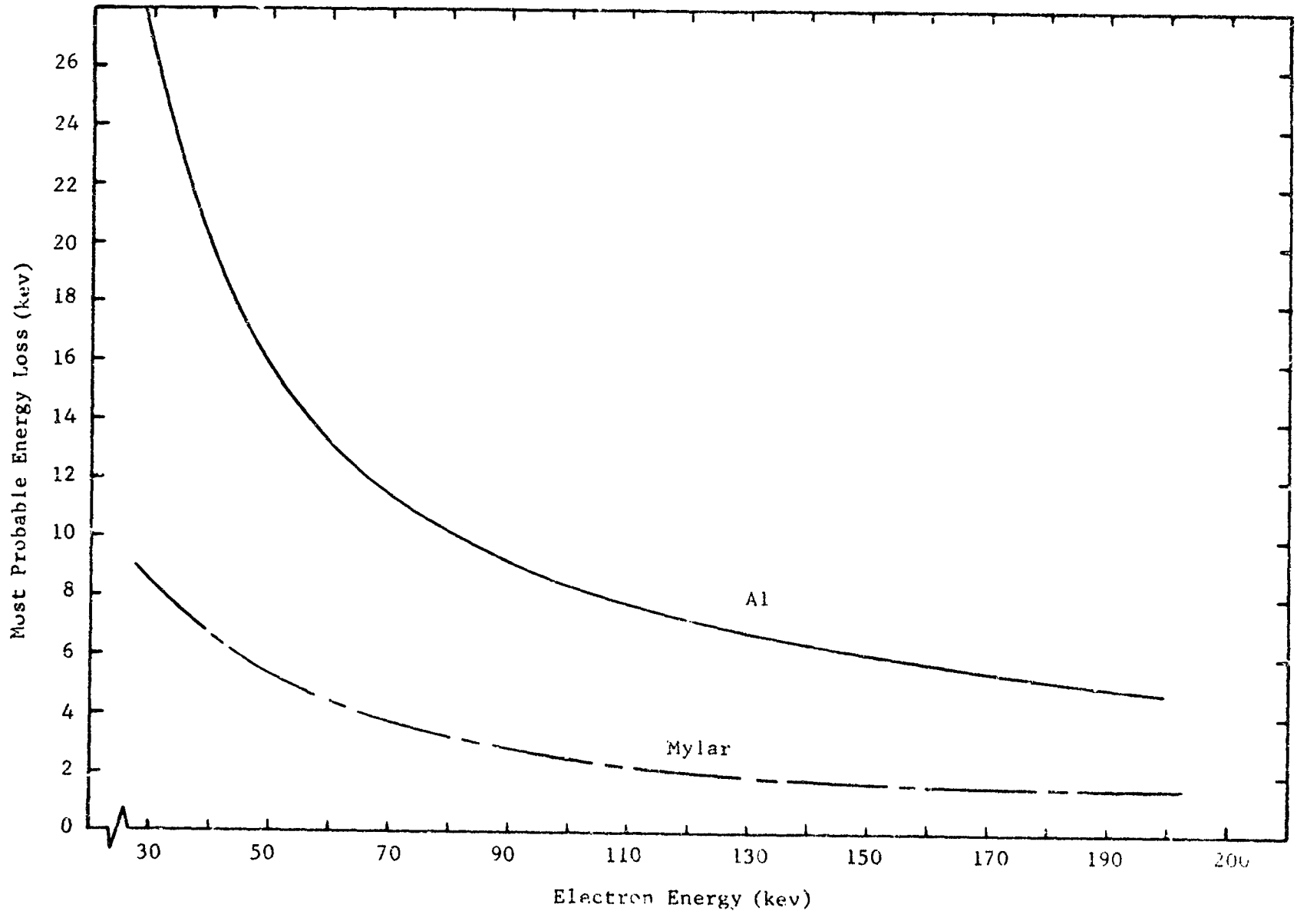

Figure 19. Most probable energy loss for electrons in 1 mil al and 1/4 mil Mylar

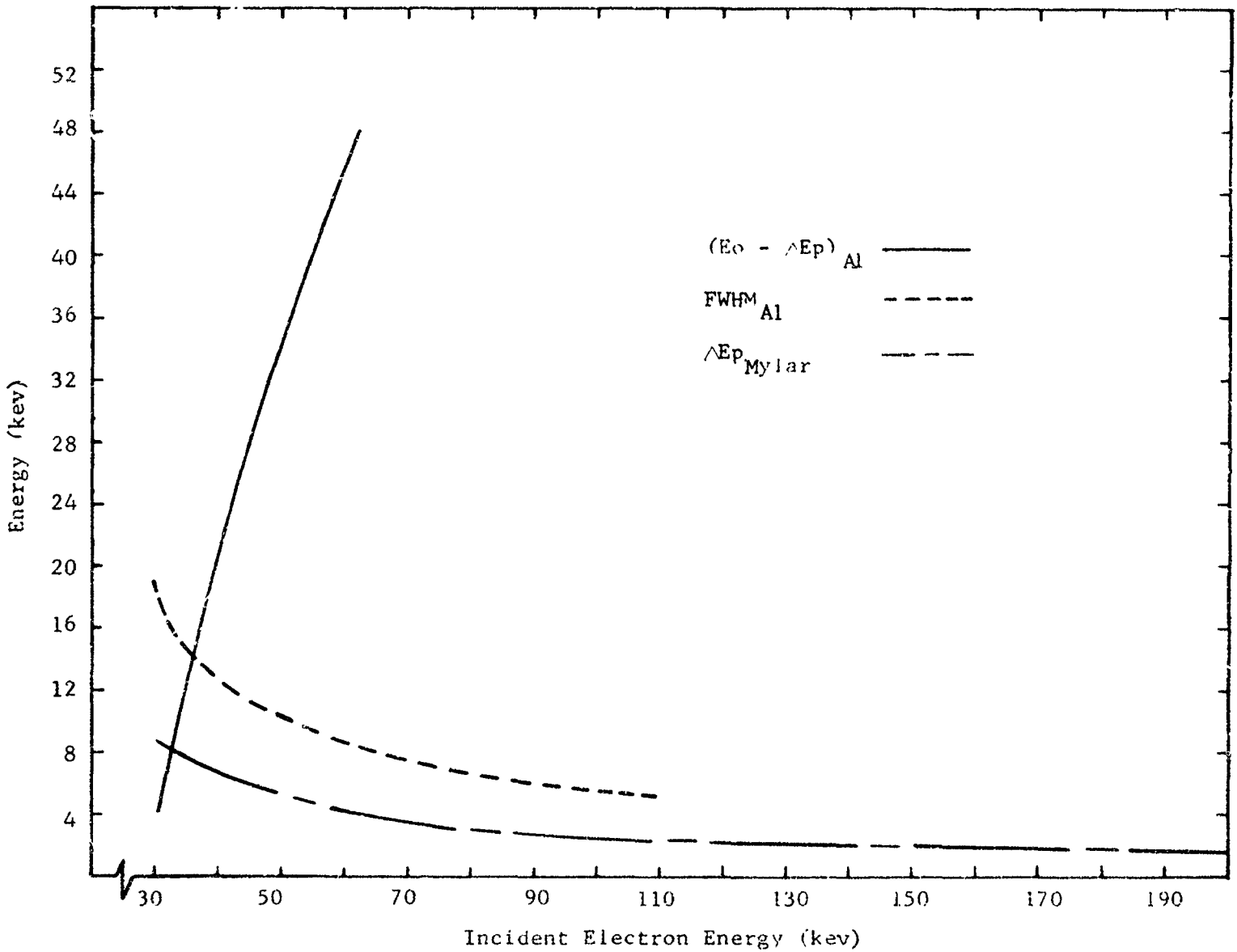

Figure 20. Most probable energy and FWHM of energy spectrum through 1 mil Al with most probable energy loss in 1/4 mil Mylar

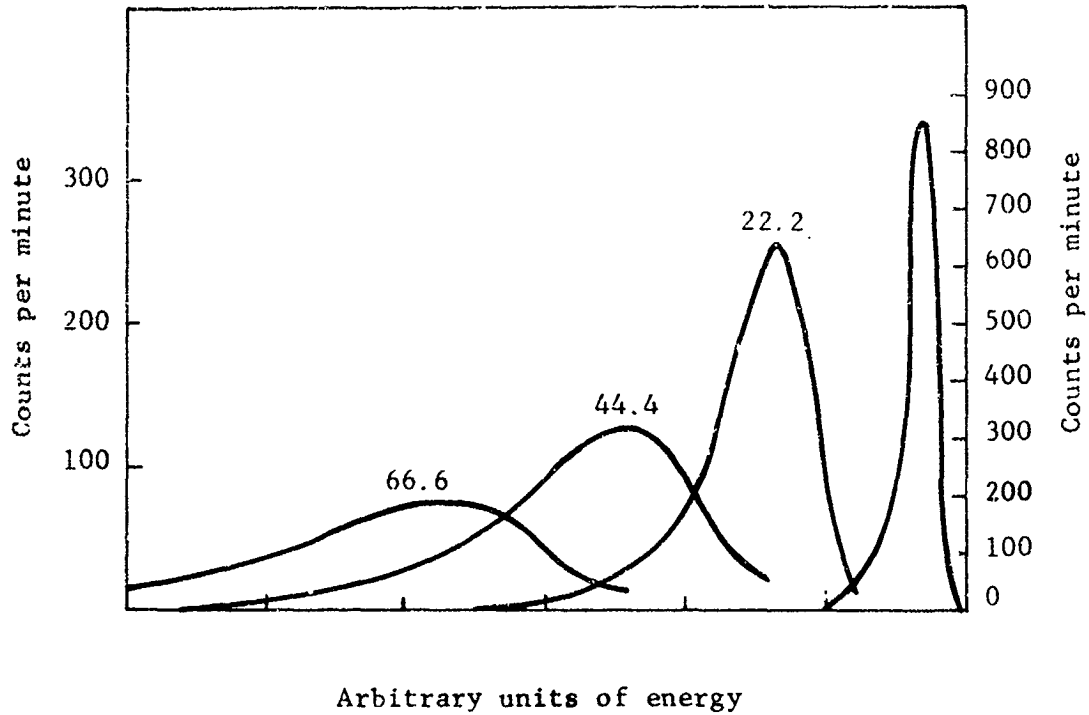

Figure 21. Straggling distribution for electrons in three thicknesses of Be where the abscissa is in arbitrary units and the ordinate is in counts per minute. The thicknesses are in mg/cm^2. The energy of the incident electrons is 624 kev.[20]

is $8 \times 10^6 \frac{\text{Mev}}{\text{cm}^2}$. These photons will have a maximum energy of 30 kev and an energy spectrum as shown in Figure 14. Therefore the attenuation coefficient will range from 2.7 cm^{-1} upward. Assuming all the x-rays penetrate 0.8 mils of aluminum, the attenuation of the x-rays with energy less than 1 kev will be attenuated more than 30% with the attenuation increasing exponentially with a decrease in energy. Therefore there will be photo electrons created throughout the one mil of aluminum as a result of stopping the 30 kev primary electrons. Presently, it is not possible to give a quantitative answer as to the number of photo electrons energetic enough to be emitted from the aluminum.

9. RADIATION EFFECTS IN MYLAR

The primary effects due to any irradiation of Mylar are induced changes in the electrical properties, structural damage and chemical changes resulting in the evolution of gases. Some of these are obviously correlated, however these correlations are either unknown or not well understood.

Radiation induced conductivity and space charge regions have been investigated in related materials. Yahagi[21] has found an increase in conductivity in a wax and explained it by a doping agent possibly acting as electron traps. In diamond the ionized electrons and holes become trapped at energy levels with sufficient lifetimes and densities to establish an appreciable internal space charge.[22,23] Adhern[24] has used alpha particle bombardment of diamond to establish an internal field corresponding to 480 volts/cm.

Although the above observations are with respect to an insulator with a well defined crystal structure, other insulating materials such as amorphous silica have yielded similar results. Pensak[25] reports on induced conductivity in various insulating materials where the results can be interpreted as resulting from ionization and an internal space-charge buildup. The effect is shown to be proportional to the amount of energy absorbed in the insulator from the electron irradiation.

Murphy[26] has observed polarization of dielectrics by electron irradiation. Occasional spontaneous discharges have been noted. The observed phenomenon cannot be interpreted in terms of macroscopic electrical properties such as volume resistivity, dielectric constant, but seems to be related to charge storage capacity due to existing traps or radiation induced traps with sufficient density and at deep enough levels to permit regions of space charge to exist for extended periods of time at room temperature. Teflon was studied, and the charge storage effect noted, however definite conclusions are lacking. From this observation one might suspect that an extrapolation to polymers would be applicable.

The work by Fowler[27] provides the most direct information about electron traps in Mylar where the analysis is based upon the energy band theory of solids. By studying x-ray induced conductivity, an electron trap density greater than 10^{17} traps/cm^3 was found. Also the decay time for the induced conductivity was measured and subsequently related to the release and recombination of electrons.

For the materials investigated, one important property becomes apparent. In materials showing a uniform distribution of traps in depth (measured in ev below conduction band), the number of traps was less than in materials with an apparent exponential distribution of trapping levels. The uniform distribution corresponded to the amorphous materials while the exponential distribution was associated with poly-crystalline materials. It is suggested that the exponential distribution

is associated with the boundaries between the crystalline regions while no explanation for the larger number of traps is offered. It is possible that this observation is an anomoly associated with the extension of the energy band theory to amorphous materials. However the effect of reduced sensitivity to radiation of amorphous materials is clearly shown by the data.

Other electrical properties of Mylar which change in a radiation environment include the dielectric constant, dc leakage resistance and dissipation factor. After exposure to a flux of 10^{16} electrons/cm^2 with a primary energy of 1 Mev, a 5 mil thickness of Mylar 2½ inches by 2½ inches showed a + 0.3% change in dielectric constant and a + 73% change in dissipation factor at 1 Kc. In addition the dc leakage resistance increased by approximately 40%.[28] Changes were also noted in the mechanical properties; in particular the stiffness in flexure and the flexural strength decreased by approximately 15%.[28]

Color changes were also noted for the flux of 10^{16} electrons/cm^2. The change was from the characteristic color of Mylar to a straw yellow.[28] Others have noted this change for both gamma and electron irradiation.[29] However, the gamma irradiated Mylar became brittle and began to crack as the yellowing began while the electron irradiated samples did not exhibit any significant brittleness. Preliminary tests indicate that the gamma irradiated sample is more crystalline than the electron irradiated sample. This significant difference could explain the variation in mechanical properties between these two forms of radiation. Although these effects represent significant changes in the properties of Mylar one must keep in mind the severity of the test to which it has been subjected. The flux for which these changes are reported is equivalent to 18 years in the Van Allen radiation belts.

10. INTERNAL SPACE CHARGE BUILDUP AND ELECTRICAL BREAKDOWN

Trapping of electrons in insulating materials has been substantiated experimentally through persistent internal polarization by irradiation of insulators under an applied bias and the investigation of thermoelectrets. It is not unreasonable to assume that the same phenomenm exists to some extent in Mylar. In view of Fowler's work one might expect that the trapped electron density can exceed 10^{17} electrons/cm^3.[27] The main problem then is to provide enough free electrons in the Mylar with an energy approaching thermal velocity. This could be accomplished by ionizing radiation such as energetic electrons or photons. Under an applied bias this leads to internal polarization. Characteristically, the internal field is less than the applied field. Also with no bias applied the net persistent internal polarization would be zero since there would be no external force to orient and separate the ionization.

Another method for achieving a large electron density in traps is to inject electrons into Mylar which then reach thermal velocity through scattering and lattice vibrations. Ionization of the Mylar is not excluded from the injected electron interactions. However, to calculate the expected space charge buildup resulting from trapped electrons the ionizing events will be neglected. Consider the simple model in Figure 22. Electrons are injected at $x = 0$, uniformly across the face of the Mylar. Furthermore, it is assumed that all of these electrons are stopped within a distance d_1 in Mylar and result in a uniform charge density ρ for $x < d_1$ and charge density zero for $x > d_1$. Therefore by Poison's equation

$$\nabla^2 V = -\frac{\rho}{\epsilon} \qquad 0 \leq x < d_1 \tag{29}$$

$$\nabla^2 V = 0 \qquad d_1 < x \leq d \quad . \tag{30}$$

By integrating these equations and applying the proper boundary conditions, one can show that the maximum value of electric field occurs at $x = 0$ for $d_1 < d$; for $d_1 = d$ the electric field is a maximum at $x = 0$ and $x = d$. The value of the maximum field, where A is the area of the capacitor electrodes, is

$$\begin{aligned} |E|_{max} &\approx \frac{\rho}{\epsilon}\frac{d_1}{d}\left(d - \frac{d_1}{2}\right) \\ &\approx \frac{qN_A}{\epsilon d}\left(d - \frac{d_1}{2}\right) \end{aligned} \tag{31}$$

Clearly the value of $|E|_{max}$ differs only by a factor of 2 as d_1 goes from $d_1 \ll d$ to $d_1 = d$ for a given number of electrons per cm^2 (N_A) in the region of charge density. For breakdown due to internal electric

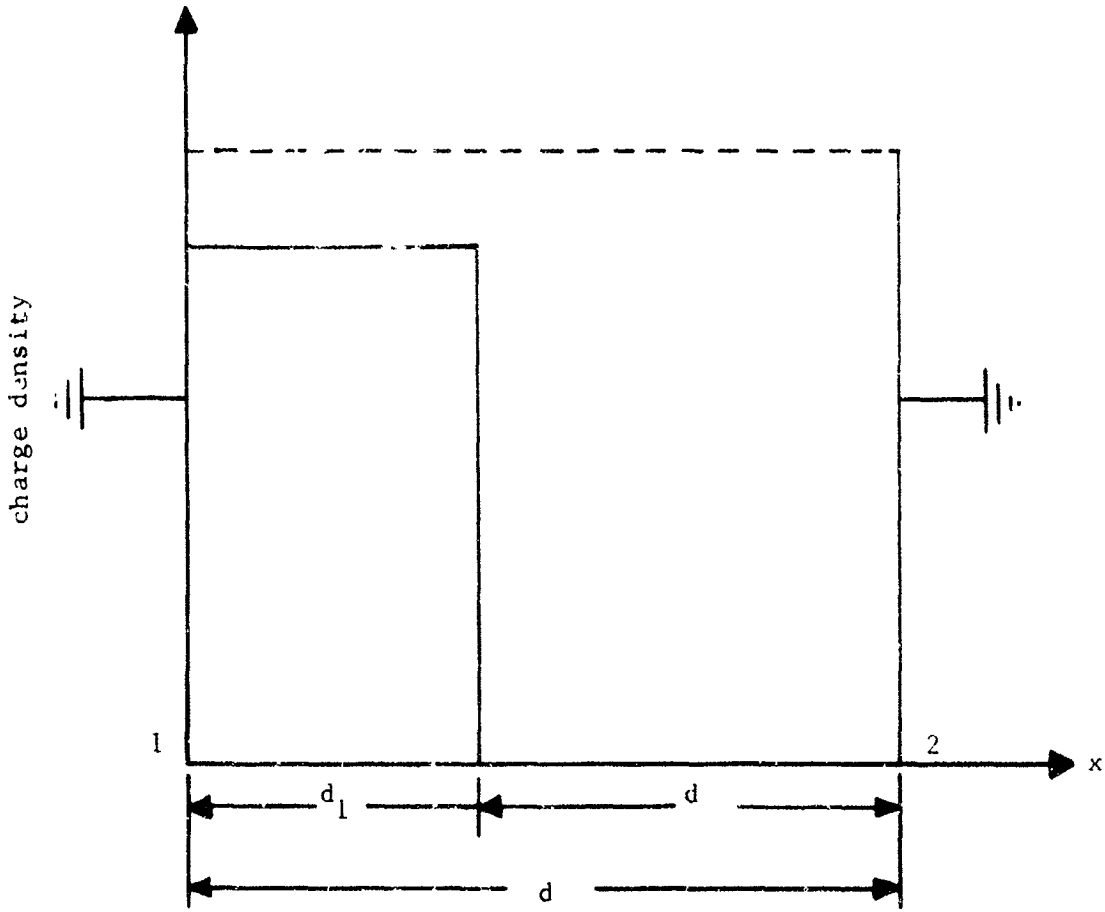

Figure 22 Assumed charge distribution in traps with boundaries 1 and 2 grounded

field only the value of $|E|_{max}$ will be considered. For the stated assumptions the maximum value of internal electric field can be related to the total number of electrons/cm^2 entering the Mylar. These relationships are developed in Appendix A and the results are plotted in Figure 23.

Due to the presence of an internal field resulting from a net trapped charge, field induced breakdown can occur. The breakdown mechanism could be either Zener or electron avalanche. The Zener breakdown depends upon the change in rate at which electrons pass from the valence band to the conduction band under the action of a constant electric field. Avalanche breakdown results when free electrons are accelerated by the constant electric field and gain more energy from the field than is given up through lattice collisions. Thus the electron is able to obtain enough energy to cause ionization and secondary electrons which result in an avalanche process. Generally it is thought that collision ionization by electrons is responsible for breakdown of solid dielectrics.[30] Quoted values for the field strength (electric field required to initiate breakdown) range from 2×10^6 v/cm to 6×10^6 volts/cm.[31, 32] These values are nearly independent of: (a) voltage transient in the range 10^{-6} to 10^3 sec, (b) temperatures ranging from -180 to 25°C, and (c) thickness in the range of 0.25 to 0.20 mils.[31] Often breakdown pulses are observed for much lower fields than those stated above. In fact Inuishi[31] has found that the most probable breakdown process at room temperature with thin films or large electrodes areas is failure at a defect. This is due to the localization of the electric field at a defect center where charge trapping occurs and to lattice irregularities which reduce the intrinsic strength of the material.

Field strength of Mylar has been shown to be sensitive to irradiation. After irradiating a 2 mil sample with a dose of 10^7 rads of 2 Mev electrons at a dose rate of 10^6 rads/min the breakdown field strength decreased by 10%.[32] This decrease is also a function of dose rate with the most pronounced change occurring at the lower dose rates.

Assuming a uniform density of trapped charge throughout the Mylar, breakdown will be initiated either where the electric field is a maximum or at a localized defect where the electric field at the defect exceeds the breakdown field strength of the region. The breakdown initiated at defects will be a random process which will depend upon the nature and location of the defect. Although this may be the primary cause of the observed pulses, it will be neglected until later.

Breakdown due to the high electric field at the boundary of the dielectric can be initiated at either surface for the ideal model of uniform charge density for $0 \leq x < d$. This can lead to either a partial or total liberation of the trapped charge. The mechanism for this charge release is either a Zener or avalanche phenomenm as described previously. However in either case the breakdown should be lower since the energy necessary to release the trapped electrons is less than for a transition from valence to conduction band. Therefore the lower breakdown after irradiating Mylar could be an indication that electron release from traps initiates an avalanche mechanism.

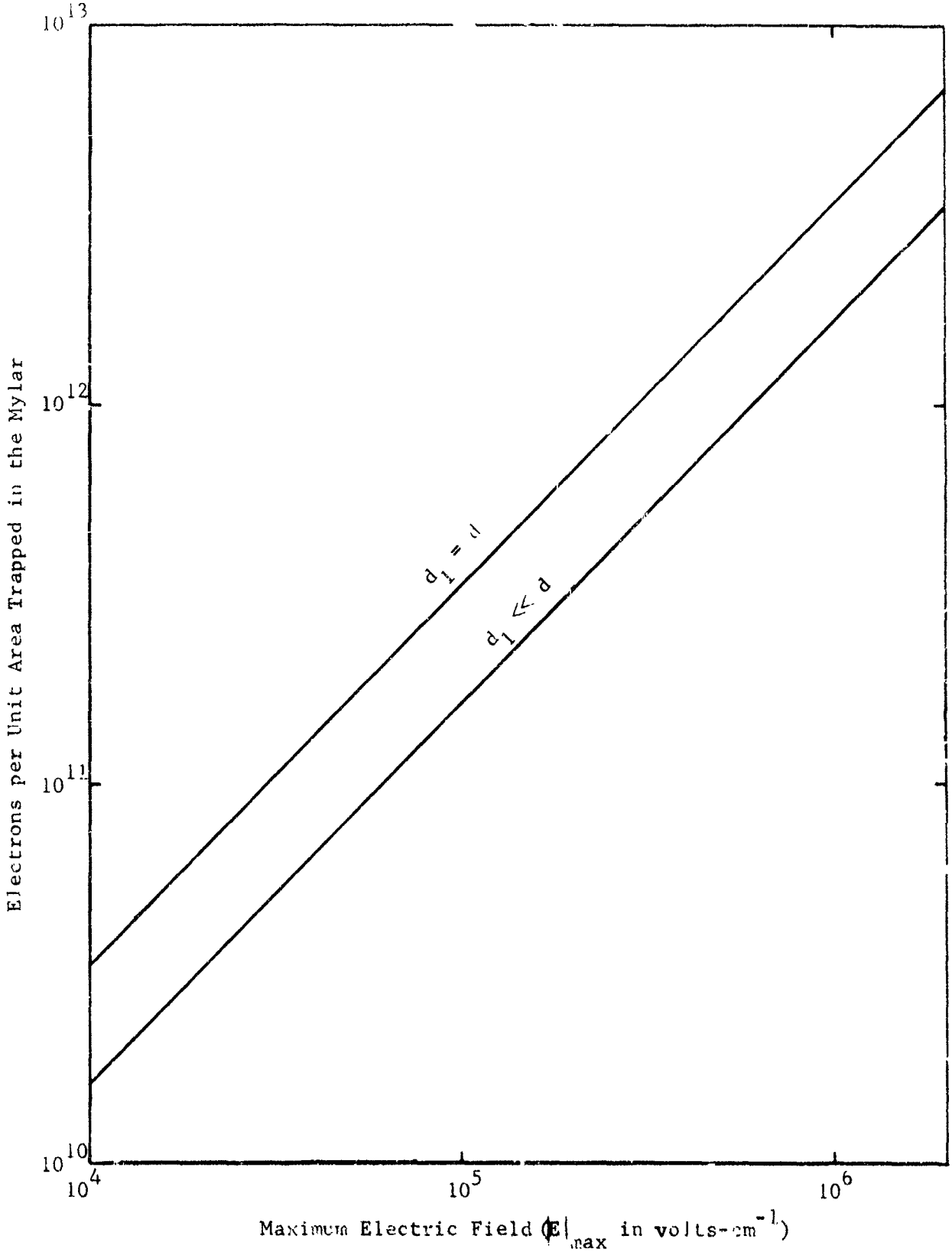

Figure 23. Maximum built-in field for a uniform electron density

The breakdown mechanism has been analyzed to this point without concern for detecting the occurrence of the trapped charge liberation. For a capacitor under bias and with a load resistor as shown in Figure 12, this analysis can be modified to evaluate trapped charge induced breakdown resulting in a transient voltage across the load resistor. The bias voltage will result in an electric field which can be added directly to that resulting from the trapped charge. For applied voltages less than 100 volts this added field will be less than 10^5 v/cm. Assuming breakdown occurs at 10^6 v/cm or greater for E_{max} the applied bias need not be considered. When E_{max} is large enough to initiate breakdown at the surface, the volume of charge liberated can range from the total charge in traps to only an infinitesimal charge layer in the region where the electric field is a maximum. However for the assumption of uniform charge density throughout the Mylar, most of the dielectric contains an electric field which is within an order of magnitude of $|E|_{max}$. Therefore it appears likely that breakdown initiated by $|E|_{max}$ will liberate most of the trapped charge.

For localized breakdown the amount of charge liberated is probably confined to the region near the defect since the remainder of the dielectric is not subjected to either the localized field or the reduced intrinsic strength associated with the defect. Therefore it is expected that defect breakdown may be approximated by assuming a variable field strength and a subsequent volume of charge liberated. To do this consider the model of internal field due to trapped charge. Assume that the trapped charge is uniformly distributed throughout the dielectric and that the field everywhere is below that of the intrinsic field strength of the material. Furthermore assume that the localized breakdown will occur at a defect and a volume of charge N_A/d_2 is liberated and recombines at plate 2. The displacement vector at electrode 1 can be obtained both before and after the liberation of the trapped charge. As developed in Appendix B this results in a surface charge difference of

$$\Delta\sigma = \sigma_E - \sigma_A = \frac{qNd}{2} - \frac{qNd_1}{d}\left(d - \frac{d_1}{2}\right) . \tag{32}$$

This represents the amount of charge transferred through the load resistor after breakdown for the capacitor electrode surface charge to reach an equilibrium value. Thus the discharge voltage across the capacitor at time t = 0+ after breakdown (assuming charge liberation occurs in zero time) is equal to

$$V_o = \frac{qN_A}{2C_A}\left(\frac{d_2}{d}\right) , \tag{33}$$

where C_A is the capacitance per unit area. This voltage also appears across R_L and a characteristic RC discharge transient results where

$$V = V_o \, e^{-t/R_L C} \, . \tag{34}$$

To evaluate the magnitude of the voltage at $t = 0^+$ one must know the value of electrons/cm^3 in traps and the portion of the charge liberated. For defect breakdown, assigning values to these quantities would be meaningless. However, after calculating the magnitude of voltage associated with breakdown initiated by E_{max} an upper limit for defect breakdown can be established.

If $d_2 = d$ in Equation (33), breakdown initiated by E_{max} can be determined. Using the value of $E_{max} \approx 10^6$ v/cm the corresponding charge in traps under the assumptions used to develop Equation (31) would be 3.4×10^{12} electrons/cm^2. For 1/4 mil Mylar the capacitance is 4.18×10^{-10} f/cm^2. Thus

$$V_{o\ max} = 1.91 \times 10^{-10} \, N_A = 600 \text{ volts} \, . \tag{35}$$

From the data presented by Langley Research Center and Marshall Space Flight Center the assumed value of $N_A = 3.4 \times 10^{12}$ electrons/cm^2 seems reasonable. Therefore the observed voltage can be written as

$$V_o = 600 \left(\frac{d_2}{d}\right) \tag{36}$$

for those cases where complete liberation of charge does not occur. For discharge pulses less than 10 volts $d_2/d \leq 0.0167$ or only a portion of the trapped charge is liberated. Clearly, a wide variation in pulse heights would be observed for defect breakdown.

Using similar arguments, the voltage pulse due to the liberation of charge that is trapped only near the aluminum-Mylar boundary at electrode 1 in Figure 22 can be calculated. If the trapped electrons are uniformly distributed for $0 \leq x < d_1$, the maximum electric field occurs at $x = 0$ and is, for $d_1 \ll d$

$$|E|_{max} = E(0) \approx \frac{qNd_1}{\epsilon} \, . \tag{37}$$

The electric field at electrode 2 is

$$|E(d)| = \frac{qNd_1^{\,2}}{2\epsilon d} \, . \tag{38}$$

Assuming that all the trapped charge is liberated in negligible time to electrode 1 when $|E|_{max}$ reaches the value necessary to initiate

breakdown, the surface charge on electrode 2 that must be transferred through the load resistor to establish equilibrium is related to the displacement vector D_2 by

$$D_2 = \epsilon E(d) = \sigma_s = \frac{-qNd_1^2}{2d} = \frac{-qN_A d_1}{2d} \quad . \tag{39}$$

Therefore the transient voltage across the capacitor at time $t = 0+$ after breakdown (assuming charge liberation in zero time) is equal to

$$V_o = \frac{-qN_A}{2C_A}\frac{d_1}{d} = -1.91 \times 10^{-10}\, N_A \frac{d_1}{d} \quad . \tag{40}$$

This voltage also appears across R_L with the characteristic RC transient of Equation (34). From Figure 23, a value of N_A can be obtained from the curve $d_1 \ll d$ to estimate the expected voltage transients. Assuming a value of $E_{max} = 10^6$ v/cm will initiate breakdown and liberate all trapped charge, the electrons per cm^2 in traps required from Figure 23 is approximately 1.6×10^{12} e/cm^2. Thus

$$V_o = 3.06 \times 10^2 \frac{d_1}{d} \text{ volts} \quad , \tag{41}$$

where d_1 is restricted to values such that $d_1 \ll d$. Therefore over the range of validity for Equation (37) the maximum value of the transient voltage is approximately

$$V_{o\ max} \leq 30.6 \text{ volts} \quad . \tag{42}$$

It is apparent from Equations (35) and (42) that trapping restricted to the region in the Mylar near electrode 1 will result in lower values of discharge pulses. Also the breakdown will occur only in one direction for this idealized model.

Extending this simple model, certain aspects of the radiation induced breakdown can be deduced. For example, it has been assumed that the release of electrons from traps happens instantaneously and yields the net surface charge in Equation (32). However the liberation of trapped charge occurs in a finite time which alters the values of voltage given in Equations (34) and (42). There will be a finite rise time for the discharge pulse with an amplitude depending upon the load resistance, the capacitance of the detector, and the rate of charge release induced by breakdown. To illustrate the dependence of the breakdown pulse on these parameters consider the case where the net surface charge increases linearly with time until all the liberated

charge has reached the electrode where the breakdown was initiated. Thus

$$\frac{\Delta\sigma_s}{\Delta t} = \tau \qquad 0 \leq t \leq T$$

where τ is net surface charge per unit time and T represents the finite time for charge liberation. The resulting voltage across the capacitor due to the net surface charge is

$$\frac{\Delta V_c}{\Delta t} = \frac{1}{C_A}\frac{\Delta\sigma_s}{\Delta t} = \frac{\tau}{C_A} \qquad 0 \leq t \leq T \tag{43}$$

where C_A is the capacitance per unit area of the detector. Using circuit analysis the voltage across the load resistor is

$$V_R(t) = \tau RA(1 - e^{-t/RC}) \ . \qquad 0 \leq t \leq T \tag{44}$$

Equation (44) has a maximum value for t = T therefore

$$V_R(t) \leq V_R(T) = \tau RA(1 - e^{-T/RC}) \ . \qquad 0 \leq t \leq T \tag{45}$$

At t = T all the liberated trapped charge has moved to electrode 2 and Equation (34) can be used for the time interval $T \leq t \leq \infty$ where V_o is replaced by $V_R(T)$. From this analysis it is evident that the amplitude of the discharge pulse depends upon the load resistance, the capacitance and the rate of charge liberation during breakdown.

11. CORRELATION OF DATA WITH THEORETICAL MODEL

The results of this simple model are in qualitative agreement with the reported observations where reproducible experiments could be performed. For example in the experiments associated with Figure 11 it was noted that the number of pulses decreased with increasing temperature for a given total dose. From the fundamental experiments cited,[26] thermal activation of trapped electrons has been used to obtain data on the number of electrons in traps. As the temperature increases, trapped electrons are activated thermally and the number of injected electrons which become trapped decreases. Therefore a larger number of injected electrons are required to achieve a charge density that will result in an electric field which can initiate breakdown.

The observation that dose rate and applied voltage (total dose held constant) have little effect upon the number of pulses is consistent with the idea that breakdown depends primarily upon the number of electrons in traps for an applied voltage less than 100 volts. Also breakdown can be initiated to either electrode for the uniform charge distribution with a maximum observable voltage of 600 volts. In establishing this maximum it was assumed that full discharge of the capacitor occurred in zero time. For a partial discharge or finite discharge time the maximum observable voltage can vary over 2 to 3 orders of magnitude. This behavior has been observed. However for these data the availability of electrons crossing the aluminum-Mylar boundary for primary energies less than 100 kev cannot be determined using either available theoretical analysis or experimental observations. A mechanism based upon photoelectrons being the primary constituent of any electron transfer across this boundary has been suggested, but experimental verification is lacking. To investigate further the pulsing at low energies, fundamental studies directed specifically at secondary electron emission from aluminum with primary energies in the range of interest must be conducted.

For the experiments associated with Figure 12, pulsing of the capacitor for primary energies ranging from 150 to 200 kev at a rate of one pulse every 5×10^{14} e/cm^2 can be qualitatively explained by this simple model. It was noted that pulsing only occurred with a back-up plate but ceased when the plate was removed. In this energy range most of the primary electrons penetrate the capacitor. As the primary beam passes through the Mylar, energy is given up which is ultimately reduced to thermal energy as the ionized and excited atoms dissipate the energy through lattice vibrations and collisions. This results in a heating of the dielectric. In a vacuum, heat transfer is rather restricted and localized heating of the detector is not unreasonable to expect. As indicated previously, the trapping of injected electrons should decrease as the temperature is increased. Therefore, without the back-up plate the increase in temperature reduces the number of injected electrons which are trapped and reduces the pulsing for a given number of primary electrons.

With a metal back-up plate the heat generated in the mylar can be redistributed throughout the back-up plate and the mylar, hence localized heating of the mylar is less likely to occur. Therefore more injected charge is trapped than for the unbacked detector. For the energy range 150 - 200 kev the secondary yield is approximately 10%, therefore for 5×10^{14} e/cm^2 in the primary beam approximately 5×10^{13} secondary electrons per cm^2 cross the boundary. Assuming a maximum electric field of 10^6 v/cm will initiate breakdown, approximately 10% of the secondary need be trapped to result in breakdown. This indicates that for the unbacked detector very few (possibly less than 1%) of the secondaries are trapped in the Mylar.

The data from Marshall Space Flight Center are certainly consistent with the results of this study in so far as they are available. However the data are continually being updated which precludes any conclusive evaluation until they are available in a convenient form. The one datum which has been reproducible and is significant with respect to this study is the average ratio of flux per pulse of 4.6×10^{12} e/cm^2. Assuming an electric field of 10^6 V/cm is necessary to initiate breakdown, there is approximately one electron trapped for each primary electron. Since the secondary yield is less than 100% for aluminum and all the primaries are not stopped in the Mylar for the energies under consideration, a combination of both primary and secondary electron trapping in the Mylar must be occurring. Due to the straggling of the primary electrons and secondary yields of approximately 10%, these results are consistent within the limits of applicability of the simple model.

27388 over

12. SUMMARY

The study of the signal generation mechanism occurring upon impact of a projectile on a capacitor-type micrometeoroid detector is carried out by formulating a model for the impact process and then using this model to suggest possible mechanisms of capacitor discharge. In the assumed model essentially one-dimensional strong shock wave theory is used to predict the impact induced thermodynamic states. It is found that these thermodynamic conditions are sufficient to produce a highly-ionized plasma in the shocked regions of the capacitor and projectile. This plasma acts like a fluid metal, being bound together by free electrons in a lattice of positive ions. It is shown that a quasi-lattice model of this type not only accounts for the formation of the plasma at temperatures much below those normally required for thermal ionization but also accounts for the impact light flash.

Two mechanisms of capacitor discharge are suggested from the results of the impact study. In the first mechanism discharge is initiated by electro-mechanical breakdown of the Mylar dielectric due to the large pressures transmitted to it by the mechanical shock. In the second mechanism the discharge is initiated and sustained by a dense plasma which is generated on impact and penetrates through the capacitor, momentarily producing a low but finite resistance path between the electrodes. In the proposed model of the signal generation mechanis either electro-mechanical breakdown or a plasma conduction path may be initiating the capacitor discharge but the plasma conduction path must be occurring to sustain the discharge.

The more significant experimental observations of the NASA are compared qualitatively with the proposed model of the signal generation mechanism and the correlation appears to be quite good.

The study of possible ambiguous signal generation is conducted through a search for data which permits evaluation of the electrical properties of the capacitor type micrometeoroid detector in a space radiation environment. Electron radiation is the primary source of concern in a space application. The number of primary and secondary electrons which either pass through or are stopped in the Mylar is considered. Fundamental data on primary electron straggling and secondary electron emission for thick absorbers indicate that a significant number of electrons are stopped in the Mylar. Also there are numerous studies investigating the trapping of electrons in Mylar. From these studies, it is suspected that there are trap densities in excess of 10^{17} traps per cm^3 and trapping lifetimes on the order of hours at room temperature. Therefore, a given injected charge which subsequently becomes trapped will yield an electric field throughout a small region of the Mylar.

A simple model is proposed for investigating and characterizing breakdown transients which are induced by electron radiation. Only general observations can be made with such a simple model, however the

results are in qualitative agreement with existing reproducible data. It is concluded that breakdown most likely occurs at a defect in the Mylar. The amplitude of the discharge transient will depend upon the nature of the defect, however a maximum observable value can be estimated. For an assumed value of 10^6 v/cm for the electric field which will initiate breakdown, a maximum amplitude of 600 volts is established for uniform charge trapping throughout the Mylar while trapping near the aluminum-Mylar boundary results in approximately a 30 volt maximum. Both of these values depend upon the assumption of trapped charge liberation in zero time. Allowing for a finite discharge time decreases the maximum amplitude. The number of electrons per cm^2 in traps in the volume of charge density which result in these breakdown characteristics is approximately 10^{12} e/cm^2. From these observations it is predicted that pulsing should not occur for integrated electron flux levels below this value.

Author

13. RECOMMENDATIONS

From the impact study it is apparent that additional experimental information is needed on the discharge characteristics of the micrometeoroid detector. This information could be obtained by two sets of experiments. The first set of experiments would be concerned with the plasma conduction mechanism of capacitor discharge. The type of plasma formed on impact would be determined and its conduction characteristics investigated. Some supplementary experimental investigations which should also be made are:

1. Determine if an impact light flash is always observed when a sustained capacitor discharge occurs.
2. Investigate the effect of polarity on both the discharge mechanism and the light flash.
3. Investigate the characteristics of the discharge under a vacuum of 10^{-7} torr. Also determine the effect of the ambient medium on the discharge voltage by conducting impact tests in air and then in a medium of lesser electron affinity such as argon or helium.

The second set of experiments would deal with the operational characteristics of the capacitor. One important experiment would be to try to correlate the discharge voltage V_d with the rate at which energy is added to the target by the projectile This would enable a determination of the effect of projectile size, density, and velocity on the discharge characteristics. It would also establish a limit on the energy input rate below which a sustained discharge would not be observed. Another experiment of importance would be to investigate the capacitor discharge characteristics when pressure-induced breakdown occurs at impact velocities that are too low to cause a sustained capacitor discharge.

As a result of the ambiguous signal generation portion of this study, it has become apparent that valuable data on the capacitor detector which will help fill the information gap may be obtained by two relatively simple experiments. The first of these employs a radioactive beta source, promethuim, for irradiation. Calculations indicate that this will allow an integrated flux comparable to that obtainable with accelerators in an economic and practical experiment. Additionally the energy spectrum is a closer simulation to the real space environment.

The primary experiments to be performed using the beta source should include a practical evaluation of the performance of a capacitor detector in a radiation environment. Suggested experiments include:

1. The 1 mil aluminum, Mylar, aluminum film structure should be irradiated and the discharge pulsing observed as a function of the integrated electron flux and the electrical parameters.
2. Similar capacitors but provided with evaporated aluminum films on both Mylar surfaces should be irradiated in order to assess the role of the adhesive normally used in bonding the Mylar to the aluminum plate.

3. Similar structures but with alternative film dielectrics should be observed for pulsing under irradiation.
4. Edge effects should be examined for various configurations.
5. Affects of thickness and geometry of capacitor elements should be examined.
6. These structures should be tested at various temperatures.

The second series of experiments utilizes a demountable x-ray tube as a mono-energetic electron source and more closely approximates accelerator experiments. However, the low energy electrons (less than 50 kev) can be readily obtained in an economical manner. These experiments should be directed toward obtaining a better understanding of the physical phenomena in the discharge processes. A demountable x-ray tube modified to use a capacitor micrometeoroid detector structure as a target will provide voltage and current levels which are adjustable over a wide range of values. These allow a different set of experiments as described below.

1. The energy spectrum of the electrons which emerge from the aluminum can be determined by a retarding field measurement with a Faraday cage.
2. Capacitors provided with evaporated aluminum films on various dielectrics including Mylar can be irradiated and the resulting net space charge or internal polarization determined.
3. Assuming a net space charge is detected, a charge sensing circuit can be used to detect the liberation of trapped charge by heating the capacitor.
4. Photoelectric activation can be used to investigate the characteristics of the electron traps.
5. The electronics used to determine the current and voltage relationship of the discharge phenomena must be considered in evaluating all data.

From this series of experiments one can obtain data which will permit a more complete and exacting model for the operational characteristics of a capacitor type micrometeoroid detector in a radiation environment.

For a uniform charge density (ρ) throughout the volume Ad_1, as shown in Figure 22, where A is the cross sectional area and d_1 the depth in the x-direction to which the charge distribution extends, Poison's equation reduces to a one-dimensional problem and

$$\frac{d^2V}{dx^2} = -\frac{\rho}{\epsilon} \qquad 0 \leq x < d_1 \ , \tag{A-1}$$

where ϵ is the absolute dielectric constant of the medium. In the region without a net charge density

$$\frac{d^2V}{dx^2} = 0 \qquad d_1 < x \leq d \ . \tag{A-2}$$

Using the boundary conditions that the potential is zero at the extreme boundaries

$$V(0) = V(d) = 0$$

and that the displacement vector is continuous across the boundary at $x = d_1$, the electric field in these two regions is

$$E = -\frac{qN}{\epsilon}\left[x - \frac{d_1}{d}\left(d - \frac{d_1}{2}\right)\right] \qquad 0 \leq x \leq d_1 \tag{A-3}$$

$$E = -\frac{qNd_1^{\,2}}{2\epsilon d} \qquad d_1 \leq x \leq d \tag{A-4}$$

where q is the electronic charge and N is the number of electrons per cm^3. For $d_1 < d$ the maximum electric field occurs at $x = 0$. Also if $d_1 \ll d$

$$E_{max} = E(0) \simeq \frac{qNd_1}{\epsilon} \ . \tag{A-5}$$

Therefore the number of electrons per cm^2 (N_A) required to yield a given value of E_{max} is

$$N_A = \frac{\epsilon E_{max}}{q} . \tag{A-6}$$

If $d_1 = d$ which requires that the charge be distributed uniformly throughout the entire volume (Ad), the maximum electric field occurs at $x = 0$ and $x = d$ and is

$$E_{max} = \frac{qNd}{2\epsilon} . \tag{A-7}$$

Again the electrons per cm^2 required to yield a given value of E_{max} can be determined by

$$N_A = \frac{2\epsilon E_{max}}{q} . \tag{A-8}$$

The results of Equation (A-6) and (A-8) for Mylar are shown in Figure 23.

APPENDIX B

To calculate the charge transferred through the load resistor due to the liberation of a volume of trapped charge consider the electric fields in Appendix A. If the breakdown occurs to electrode number 2 and removes a volume Ad_2 where A is the area of the capacitor, of trapped electrons in Figure 22, one can calculate the surface charge on electrode 1 before and after breakdown using Equation (A-3). If the liberated charge is assumed to be liberated and recombines at electrode number 2 in zero time the difference between the values of surface charge before and after breakdown on electrode number 1 represents the charge which must be transferred from electrode 1 to electrode 2 to reach an equilibrium state of charge distribution. Since the displacement vector component D_x is continuous across the boundary at $x = 0$ the surface charge before breakdown (σ_B) on electrode 1 is

$$\sigma_B = D_x(0)_B = \epsilon E_{max_B} = \frac{qNd}{2} . \tag{B-1}$$

For the stated assumptions the surface charge after breakdown (σ_A) at electrode 1 is

$$\sigma_A = D_x(0)_A = \epsilon E_{max_A} = qN\left[\frac{d_1}{d}\left(d - \frac{d_1}{2}\right)\right] . \tag{B-2}$$

Therefore the net surface charge which must be transferred from electrode 1 to electrode 2 is

$$\begin{aligned} \sigma_s = \sigma_B = \sigma_A &= \frac{qNd}{2} - \frac{qNd_1}{d}\left(d - \frac{d_1}{2}\right) \\ &= \frac{qN_A}{2} - \frac{qN_A}{d}\left(d - \frac{d_1}{2}\right) \end{aligned} \tag{B-3}$$

At the time $t = 0+$ the voltage across the capacitor due to the net surface charge can be found from

$$\sigma_s = \frac{Q}{A} = \frac{C}{A} V$$

or

$$\left|V_c(0)\right| = \frac{qN_A}{2C_A} \frac{d_2}{d} \tag{B-4}$$

where C_A is the capacitance per unit area. Introducing N_A the number of electrons per cm^2 in traps, for 1/4 mil Mylar Equation (B-4) reduces to

$$\left| V_c(0) \right| = 1.91 \times 10^{-10} \, N_A \frac{d_2}{d} \qquad \text{(B-6)}$$

APPENDIX C

To investigate the large area capacitor and its electrical characteristics with respect to signal transmission, consider the ratio of capacitor area to the area where the discharge signal originates. Assuming the penetration is circular and the transfer of charge from one electrode to the other occurs uniformly about the circular symmetry, the signal current will flow radially about the discharge toward the boundary of the capacitor. Depending upon the boundary geometry, the initial radial current flow will be modified as the current lines approach the boundary.

Since the area of the capacitor is orders of magnitude larger than that of the area associated with the penetration, circular symmetry can be used near the origin of the signal source. Also, the series resistance per unit length varies as

$$R_\ell = \frac{\rho}{2\pi r t} \qquad \text{(C-1)}$$

where ρ is the resistivity and t the thickness of the metal electrode. Since the series resistance per unit length decreases as 1/r, the principal region of interest with respect to a decrease in discharge signal energy is near the origin of the signal source. Therefore a simple approximation to the problem of signal transmission from the origin of discharge to the boundary of a large area capacitor can be realized by assuming a circular capacitor with infinite extension. Practically, this implies that a finite boundary can be used if matched to the medium outside the boundary.

For the assumptions stated above and assuming inductance of the electrodes and leakage conductance through the dielectric are negligible the transmission line equations for a steady state solution reduce to

$$\frac{d^2E}{dr^2} - \frac{1}{R_\ell}\frac{dR_\ell}{dr}\frac{dE}{dr} - jwR_\ell C_\ell E = 0 \qquad \text{(C-2)}$$

where E = E(r) is the signal voltage radially from the discharge origin, R_ℓ the resistance per unit radial length and C_ℓ the capacitance per unit radial length. R_ℓ has been previously defined and C_ℓ is

$$C_\ell = \frac{\epsilon 2\pi r}{d} \qquad \text{(C-3)}$$

where ϵ is the absolute dielectric constant and d the thickness of the Mylar. Substituting Equations (C-1) and (C-3) into (C-2) and defining $\gamma = w\rho\epsilon/td$ yields

$$\frac{d^2E}{dr^2} - \frac{1}{r}\frac{dE}{dr} - j\, r^2 E = 0 \,. \tag{C-4}$$

A change of variables where $\gamma r = \xi$ yields

$$\frac{d^2E}{d\xi^2} + \frac{1}{\xi}\frac{dE}{d\xi} - j\, E = 0 \,. \tag{C-5}$$

This is a Bessel differential equation with solutions of the form[33]

$$E = C_1 J_o(\sqrt{-j}\ \xi) + C_2\, H_o^1(\sqrt{-i}\ \xi) \,. \tag{C-6}$$

Applying the boundary conditions that $E = E_o$ at $r = r_o$ the boundary of the discharge signal source and $E \longrightarrow 0$ as $r \longrightarrow \infty$, results in a solution[33]

$$E = E_o \frac{\mathrm{her}(\gamma r) + i\ \mathrm{hei}(\gamma r)}{\mathrm{her}(\gamma r_o) + i\ \mathrm{hei}(\gamma r_o)} \tag{C-7}$$

To calculate the power density spectrum of an output signal for a given discharge signal input one needs

$$|E|^2 = |E_o|^2 \frac{|\mathrm{her}(\gamma r) + i\ \mathrm{hei}\ (\gamma r)|^2}{|\mathrm{her}(\gamma r_o) + i\ \mathrm{hei}(\gamma r_o)|} \tag{C-8}$$

To evaluate the energy pass band for this transmission line equivalent of a large area capacitor a typical value of (γr_o) must be determined. For this study typical values of the parameters which make up γ are:

$$\rho_{al} = 2.8 \times 10^{-6} \text{ ohm-cm} \qquad d = 6.3 \times 10^{-4} \text{ cm}$$

$$\epsilon = 26.5 \times 10^{-14} \text{ farads/cm} \qquad t = 50 \times 10^{-6} \text{ cm} \,.$$

This results in $\gamma \simeq 10^{-5} f^{1/2}$ where f is frequency in cycles per second. Assuming a typical value of $r_o = 10^{-2}$ cm, $(\gamma r_o) \simeq 10^{-7} f^{1/2}$. Using the approximation for $\mathrm{hei}(\gamma r_o)$ when γr_o is near zero and for frequencies less than 10^{10} cps Equation (C-8) reduces to

$$\left|E\right|^2 = \left|E_o\right|^2 \frac{\left|\mathrm{ber}(\gamma r) + i\ \mathrm{bei}(\gamma r)\right|^2}{\left|2\pi\ \mathrm{hi}(\frac{\nu\gamma r_o}{2})\right|^2} \tag{C-9}$$

where ν is Euler's constant and is equal to 1.78. These results are shown plotted in Figure (C-1) for 3 radii from the point where the penetration event takes place to the boundary of the capacitor. Therefore this represents the power pass band as a function of the distance the discharge signal must travel to the capacitor bounday.

To determine the effect of this equivalent transmission line upon the discharge signal consider an exponential pulse shown in Figure (C-2) of height V_d and time constant α originating at the penetration site. Through Fourier analysis of this pulse the power density spectrum is

$$\left|F(w)\right|^2 = (\frac{V_d}{2\pi})^2 \left|\int_o^\infty e^{-(1/\alpha + jw)t}\ dt\right|^2 . \tag{C-10}$$

Evaluating the integral yields

$$\left|F(w)\right|^2 = (\frac{V_d}{2\pi})^2 \frac{1}{(1/\alpha)^2 + w^2} . \tag{C-11}$$

This result is also shown in Figure (C-3).

The energy desnity spectrum at the boundary of the circular capacitor is $\left|E_{out}\right|^2 = \left|F(w)\right|^2 \left|E\right|^2$. For the examples in Figures (C-1) and (C-3) both $\left|F(w)\right|^2$ and $\left|E\right|^2$ are relatively constant up to 10^4 cps. Therefore an estimate of the energy loss in signal transmission from the origin of the discharge to the boundary can be obtained by considering the average value of $\left|E\right|^2$ over the frequency interval to 10^4 cps. For a penetration of radius 0.01 cm within 0.1 cm of the boundary a maximum of 1.6 db of signal energy is lost in reaching the boundary. If a penetration of the same radius is within 1 cm of the boundary a maximum of 3.5db of signal energy is lost in reaching the boundary and within 10 cm a maximum of 6db is lost. In terms of the amplitude spectrum of the output pulse, the signal amplitudes at the boundary of the capacitor will be 0.83, 0.66 and 0.50 the discharge signal amplitude for the three signal transmission radii respectively. Also the falloff of $\left|E\right|^2$ at the high frequencies indicates that the output pulse will have a finite rise time. Although these calculations are for a specific penetration radius (10^{-2} cm), and transmission radii of 0.1, 1; and 10 cm this analysis can be extended to smaller penetration radii. If the transmission radii remain unchanged the power loss for each transmission path will be greater the smaller the penetration radii and will result in a significant power loss in the transmission path for the model analyzed.

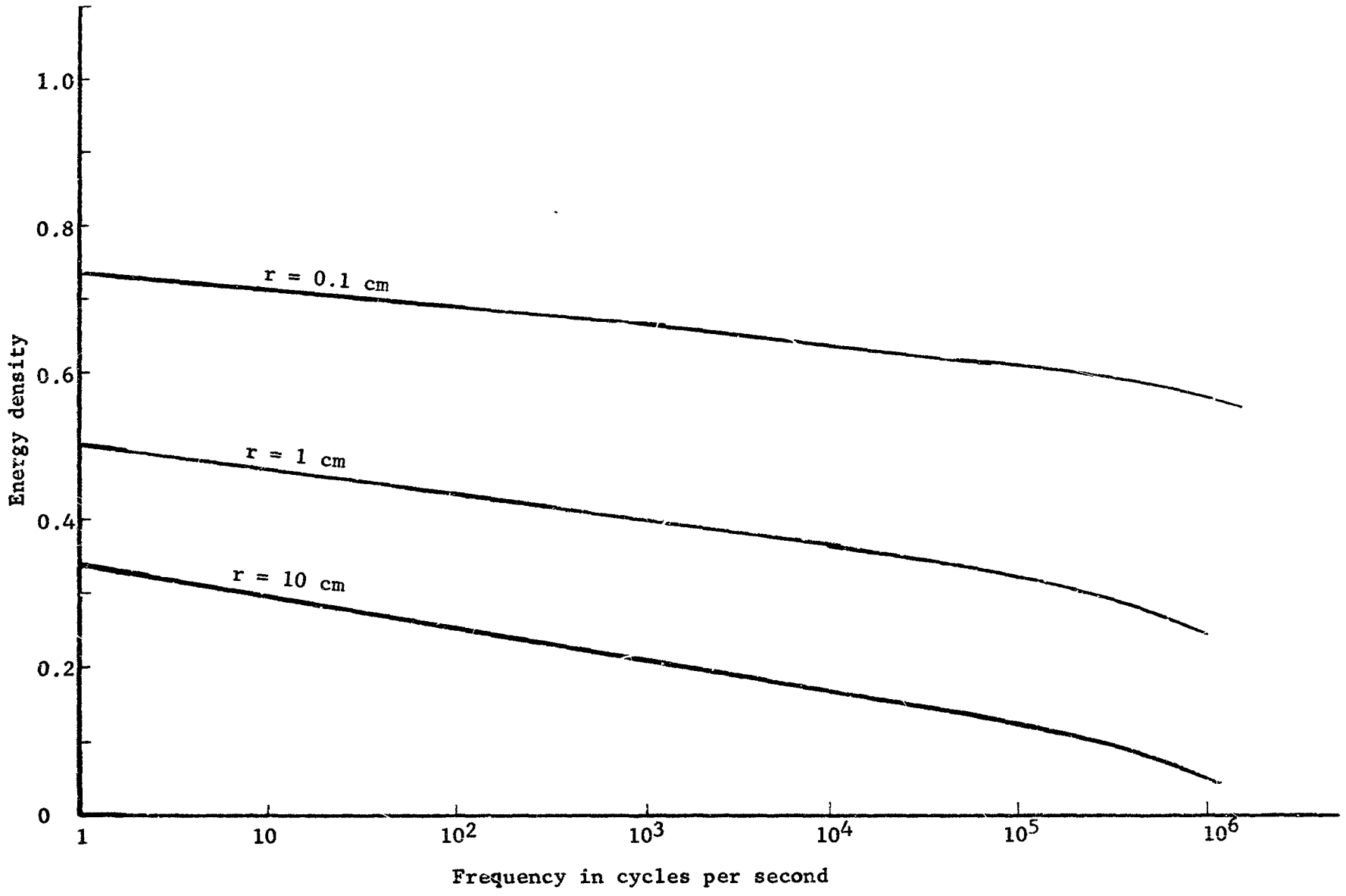

Figure C-1. Energy pass band for the cylindrical transmission line model with 3 transmission path lengths of 0.1, 1, and 10 cm

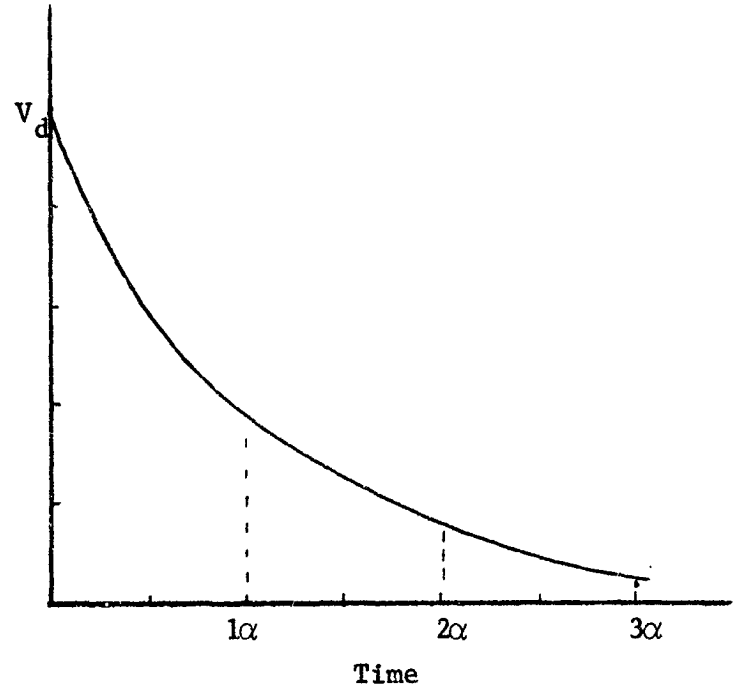

Figure C-2. Discharge signal originating at penetration radius r_0

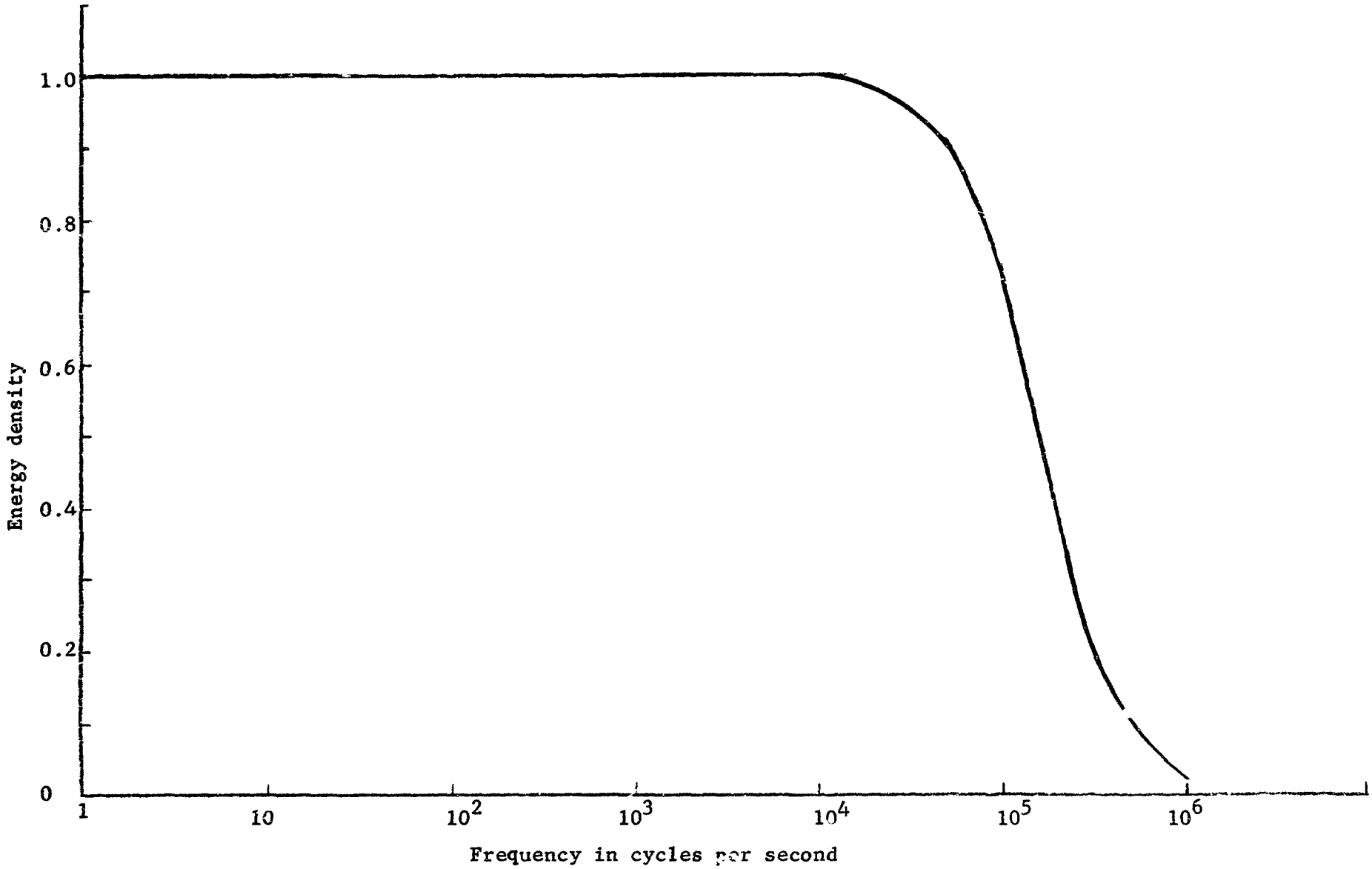

Figure C-3. Power density spectrum for an exponential signal shown in Figure 2

REFERENCES

1 - Proceedings of the Symposium on the Protection Against Radiation Hazards in Space, at Gatlinburg, Tennessee, November 5-7, 1962, N63-15138.

2 - Jet Propulsion Laboratory, "Behavior of Materials in Space Environments," L. D. Jaffe and J. B. R. Henhouse, Report No. 32-150, Contract No. NASw-6, Pasadena, California, November 1, 1961, AD 266 548.

3 - Aerojet General Corporation, "Rockets in Space Environment Vol II - The Space Environment," N. A. Williams and D. Christensen, Report No. 2484 (Final Report) Contract No. AF 04(611)-7441, Azusa, California, February 1963, N63-21000.

4 - R. J. Einchelberger and J. W. Gehring, American Rocket Society Journal, pp. 1583-1591, October 1962.

5 - K. P. Stanyukovich, Unsteady Motion of Continuous Media, Pergamon Press, New York, 1960.

6 - Arthur D. Little, Inc., On the Impact of Pellets with Thin Plates. Theoretical Considerations Part I by G. V. Bull, A. D. Little Report No. 63270-02-01, Contract No. NAS5-664, January 1962 (U) AD 273 236.

7 - Ballistics Research Laboratories, Effects of Meteoroid Impacts on Space Vehicles by R. J. Eichelberger and J. W. Gehring, BRL Report No. 1155, Aberdeen Proving Ground, Maryland, December 1961 (U) AD 272 340.

8 - M. A. Cook and W. S. McEwan, "Cohesion in Plasma," J. Appl. Phys. 29, November 1958, pp. 1612-1613.

9 - M. A. Cook, The Science of High Explosives, Reinhold Publishing Corporation, New York, 1958.

10 - Space Technology Laboratories, Inc., Study of Crater Physics by J. F. Friichtenicht, Report No. 8980-003-RU-000 Final Report, Contract No. NAS5-763, Canoga Park, California, July 1961 (U) AD 269 129.

11 - Space Technology Laboratories, Inc., Ionization Associated with Hypervelocity Impact by J. F. Friichtenicht and J. C. Slattery, Report No. 8699-6002-RU-000, Contract No. NASw-561, Redondo Beach, California, March 1963 (U) N63-15412.

12 - M. A. Cook, R. T. Keyes, and L. L. Udy, "Propagation Characteristics of Detonation-generated Plasmas," J. Appl. Phys. 30, December 1959, pp. 1881-1892.

13 - A. Bauer, M. A. Cook, and R. J. Keyes, "Detonation-generated Plasmas," Proc. Roy. Soc. A. 259, 1961, pp. 508-517.

14 - Evans, The Atomic Nucleus, McGraw-Hill, 1955.

15 - A. A. Schultz and M. A. Pomerantz, "Secondary Electron Emission Produced by Relativistic Primary Electrons," Phys. Rev. 130, 1963, pp. 2135-2155.

16 - L. Katz and A. S. Penfold, Revs. Mod. Phys. 24, 28 (1952).

17 - E. J Williams, Proc. Roy. Soc. (London), A125, 420 (1929).

18 - L. Landau, J. Phys. (USSR), 8, 201 (1944).

19 - O. Blunck and S. Leisegang, Z. Physik, 128, 500 (1950).

20 - F. Kalil and R. D. Birkhoff, "Straggling Distributions for Electrons in Passing through Thin Foils, Phys. Rev. 91, (1953), pp. 505-509.

21 - K. Yahagi, JAP 34, 804 (1963).

22 - K. G. McKay, Phys. Rev. 77, 816 (1950).

23 - A. G. Chynoweth, Phys. Rev. 83, 254, (1951).

24 - A. J. Ahearn, Phys. Rev. 73, 1113 (1948).

25 - L. Pensak, Phys. Rev. 75, 472, (1949).

26 - P. V. Murphy, JAP 34, 2061, (1963).

27 - J. F. Fowler, Proc. Royal Soc., A236, 464, (1956)

28 - J. V. Pascale, et.al, Modern Plastics, October, 1963.

29 - Dr. D. T. Turner, Research Triangle Institute, Private Communications.

30 - S. M. Kirov Tomsic Polytechnic Institute, "On the Mechanism of the Electric Breakdown of Solid Dielectrics," G. A. Vorob'yev, USSR, October 1960, N63-13621.

31 - Y. Inuishi and D. A. Powers, "Electric Breakdown and Conduction Through Mylar Films, JAP 28, pp. 1017-1022, (1957).

32 - Emanuel L. Brancato and James G. Allard, "Effects of Electron Irradiation on the Electrical Properties of Mylar."

33 - E. Janke, et.al, Tables of Higher Functions, New York, McGraw-Hill, (1960).